SorCS2 dynamically interacts with TrkB and GluN2B to control neurotransmission and Huntington's disease progression

Alena Salašová[1,2*], Niels Sanderhoff Degn[1,2*], Mikhail Paveliev[1,2+], Niels Kjærgaard Madsen[1,2+], Saray López Benito[6], Plinio Casarotto[5], Peter Lund Ovesen[1,2], Benedicte Vestergaard[1,2], Andreea Cornelia Udrea[1,2], Lilian Kisiswa[1,2], Lucie Woloszczuková[1,2], Islam Faress [1,2,3], Sadegh Nabavi[1,2,3], Eero Castrén[5], Juan Carlos Arévalo[6,7], Mai Marie Holm[8], Mads Fuglsang Kjølby[1,2], Ulrik Bølcho[1,2], Anders Nykjaer[1,2,9#].

[1)] Danish Research Institute of Translational Neuroscience, Nordic-EMBL Partnership for Molecular Medicine, Department of Biomedicine, Aarhus University, Denmark

[2)] The Danish National Research Foundation Center PROMEMO, Aarhus University, Denmark

[3)] Department of Molecular Biology and Genetics, Aarhus University, Denmark

[4)] Department of Molecular Medicine, Aarhus University Hospital, Denmark

[5)] Neuroscience Center - HiLife, University of Helsinki, Finland

[6)] Department of Cell Biology and Pathology, Instituto de Neurociencias de Castilla y León (INCyL), Universidad de Salamanca, Salamanca, Spain

[7)] Institute of Biomedical Research of Salamanca (IBSAL), Salamanca, Spain

[8)] Department of Biomedicine, Aarhus University, Denmark

[9)] Department of Neurosurgery, Aarhus University Hospital, Denmark

23 *) shared first-author

24 +) shared second-author

25 #) the corresponding author, contact information:

26 Prof. Anders Nykjaer

27 Department of Biomedicine

28 Hoegh-Guldbergsgade 10, Bldg. 1115-1116

29 Aarhus University

30 DK-8000 Aarhus

31 Denmark

32 E-mail: an@biomed.au.dk

33 Phone: +45 2899 2384

34 KEYWORDS: SorCS2, TrkB, GluN2B, BDNF, striatum, medium spiny neurons, long-term potentiation,

35 Huntington's disease

36

37

38

39

40

41

ABSTRACT

Background: Huntington's disease (HD) is a fatal neurodegenerative disorder characterized by progressive motor dysfunction and loss of medium spiny neurons (MSNs) in dorsal striatum. Brain-derived neurotrophic factor (BDNF) sustains functionality and integrity of MSNs, and thus reduced BDNF signaling is integral to the disease. Mutations in BDNF receptor SorCS2 were recently identified in HD patients. Our study investigates the role of SorCS2 in MSNs biology and in HD progression.

Methods: We derived a double transgenic line by crossbreeding SorCS2 deficient (KO) mice with the HD mouse model R6/1. Subsequently, we characterized the SorCS2 KO; R6/1 line by a set of behavioral and biochemical studies to evaluate phenotypes related to HD. Moreover, in combination with electrophysiology and super resolution microscopy techniques, we addressed the molecular mechanism by which SorCS2 controls synaptic activity in MSNs neurons.

Results: We show that SorCS2 is expressed in MSNs with reduced levels in R6/1 HD model, and that SorCS2 deficiency exacerbates the disease progression in R6/1 mice. Furthermore, we find that SorCS2 binds TrkB and the NMDA receptor subunit GluN2B, which is required to control neurotransmission in corticostriatal synapses. While BDNF stimulates SorCS2-TrkB complex formation to enable TrkB signaling, it disengages SorCS2 from GluN2B, leading to enrichment of the subunit at postsynaptic densities. Consequently, long-term potentiation (LTP) is abolished in SorCS2 deficient mice, despite increased striatal TrkB and unaltered BDNF expression. However, the addition of exogenous BDNF rescues the phenotype. Finally, GluN2B, but not GluN2A, currents are also severely impaired in the SorCS2 KO mice.

Conclusions: We formulate a novel molecular mechanism by which SorCS2 acts as a molecular switch. SorCS2 targets TrkB and GluN2B into postsynaptic densities to enable BDNF signaling and NMDAR dependent neurotransmission in the dorsal striatum. Remarkably, the binding between SorCS2 and TrkB or GluN2B, respectively, is mutually exclusive and controlled by BDNF. This mechanism provides an

65 explanation why deficient SorCS2 signaling severely aggravates HD progression in mice. Moreover, we
66 provide evidence that this finding might represent a general mechanism of SorCS2 signaling found in other
67 brain areas, thus increasing its relevance for other neurological and psychiatric impairments.

68

69

70 INTRODUCTION

71 Huntington's disease (HD) is a devastating monogenic neurodegenerative disease characterized by
72 advancing motor dysfunction, cognitive impairments, and psychiatric symptoms, which ultimately lead to
73 the death of the patient [1, 2]. HD symptoms are caused by progressive neurodegeneration of GABAergic
74 medium spiny neurons (MSNs) in dorsal striatum, which is followed by striatal and cortical atrophy [3, 4].
75 Genetically, HD patients carry an unstable CAG repeat expansion in exon 1 of the gene encoding
76 Huntingtin protein (HTT) which translates into an abnormal N-terminal polyglutamine tract resulting in
77 mutated Huntingtin protein (mHTT). In the healthy organism, HTT plays many important roles in
78 neurogenesis, intracellular protein trafficking, and synapse morphology and plasticity [1, 2]. Accordingly,
79 the accumulation of cytotoxic mHTT results in several deleterious effects such as reduced trophic
80 stimulation and perturbed synaptic plasticity, as well as diminished synaptic delivery of N-methyl-D-
81 aspartate (NMDA) receptors favoring their extrasynaptic accumulation. These abnormalities impair local
82 neurotransmission while at the same time predispose MSNs to glutamate-induced excitotoxicity [2, 5-11].

83

84 Reduced levels of brain-derived neurotrophic factor (BDNF) in dorsal striatum and its impaired
85 downstream signalling have been considered central to the altered plasticity and vulnerability of MSNs in
86 HD [12, 13]. Through the binding to the receptor Tropomyosin related kinase receptor B (TrkB), BDNF
87 triggers TrkB phosphorylation and activates manifold of intercellular signaling cascades that control

88 diverse biological functions. In the mature nervous system, TrkB activation regulates neuronal survival
89 and synaptic plasticity such as consolidation of long-term synaptic potentiation (LTP) [14-16]. For the LTP
90 to occur, TrkB must phosphorylate the N-methyl-D-aspartate (NMDA) receptor subunits GluN2B to
91 mediate GluN2B translocation into the synapse, and to increase the proportion of NMDA receptors that
92 contain this subunit [17-19].
93
94 Unlike neurons in many other brain areas, striatal MSNs do not produce BDNF [20, 21] but instead depend
95 on the BDNF release from their corticostriatal afferents [12, 22]. In mouse models of HD, reduced levels
96 of BDNF [23] and/or TrkB [24, 25] accelerate the behavioral and pathological changes, whereas cortical
97 overexpression of BDNF ameliorates the symptoms [26, 27]. The impaired BDNF-TrkB signalling has been
98 mostly attributed to the reduced delivery of BDNF to the striatum due to transcriptional repression of
99 cortical BDNF expression [5, 12], and dysfunctional anterograde axonal transport [6]. More recent studies
100 reported that in some HD mouse models, TrkB [28] and BDNF [8] levels are normal in young symptomatic
101 mice, but that TrkB does not properly activate the signalling pathways controlling potentiation at
102 corticostriatal synapses. Hence, the abnormal neurotransmission is probably important at the earlier
103 stages of HD progression, while later on, reduced trophic signalling renders the neurons vulnerable, e.g.
104 to excitotoxicity from increased extrasynaptic glutamate stimulation.
105
106 The primary determinant of HD onset is the length of the CAG repeats on the expanded allele. Yet, this
107 only accounts for 50-70% variations at the age of onset. These observations suggest the existence of
108 genetic modifiers, which remain largely unknown [1, 2, 11, 29-31]. A recent genome wide association
109 study (GWAS) of human and rat HD samples identified several single nucleotide polymorphisms (SNPs) in
110 the Sortilin Related VPS10 Domain Containing Receptor 2 (*SORCS2)* gene [32]. SorCS2 is a member of the
111 Vps10p-domain receptor family, so-called sortilins that are enriched in distinct neuronal populations.

112 Receptors of this family regulate several aspects of neuronal survival, neurodevelopment, synapse
113 remodelling, and synaptic plasticity. When dysfunctional, they are often causative to psychiatric and
114 neurodegenerative disorders [33-36]. Conceptually, these receptors function by a dual mode of action;
115 they can mediate intracellular sorting of ligands and co-receptors, and they can form complexes with
116 signalling receptors at the plasma membrane to control their activity [36].
117
118 We previously discovered SorCS2 is required for BDNF-dependent plasticity in hippocampus [33]. We thus
119 hypothesized that SorCS2 modulates BDNF-TrkB signalling in the dorsal striatum, and when absent, it
120 could aggravate HD-related symptoms in R6/1 mice. Indeed, we found that SorCS2 deficiency severely
121 worsens the motor symptoms present in the HD mice. Here we present a new molecular mechanism of
122 BDNF-TrkB-SorCS2 signaling axis, and its implication in MSN plasticity, and HD progression. We show that
123 SorCS2 enables TrkB activation and the synaptic translocation of GluN2B to MSNs synapses. While BDNF
124 stimulates the formation of a complex between SorCS2 and TrkB to boost BDNF-TrkB signalling capacity,
125 it uncouples SorCS2 from GluN2B resulting in enrichment of the neurotransmitter receptor in postsynaptic
126 densities. Given that symptomatic HD mice have reduced SorCS2 levels, the attenuated activity of the
127 receptor may be fundamental to the perturbations in synaptic plasticity that typifies HD.

128 METHODS

129 Mice

130 All mice were bred and group-housed with their littermates at Aarhus University Animal Facility with
131 unlimited access to food and water and a 12/12 hour light/dark cycle. Generation of the SorCS2 KO mice
132 is described in [37]. SorCS2 KO line has been backcrossed for ten generations into C57BL/6J, as were WT
133 mice. The R6/1 mouse model (obtained from the Jackson Laboratory, USA) was originally created on a
134 CBA/C57BL/6 hybrid background [38], but has since been backcrossed for ten generations into C57BL/6J

135 [39]. R6/1 mice were maintained on the C57BL/6J background by crossing heterozygous males with WT
136 females since R6/1 females are infertile. R6/1 mice were crossed into our SorCS2 KO mouse line to obtain
137 SorCS2 KO; R6/1 line. Mice were genotyped for *Sorcs2* and HDexon1 by PCR.
138

139 **Behavioral testing**

140 *Screening for body weight, clasping and grip strength:* We used WT, SorCS2 KO and R6/1 littermates as
141 controls to SorCS2 KO; R6/1 mice. Number of mice used: WT (11 males, 10 females), SorCS2 KO (11 males,
142 15 females), R6/1 (12 males, 16 females), and SorCS2 KO; R6/1 mice (16 males, 8 females). Out of this
143 cohort, two R6/1 males (both 22 weeks old) and two R6/1 females died (17 weeks and 19 weeks old).
144 Three of the R6/1, SorCS2 KO males (two 18 weeks old and one 21 weeks old) and one SorCS2 KO; R6/1
145 female died (17 weeks old). Data from these death individuals are included in the graphs until the last age
146 they were tested. The experiments were double-blinded. Mice were tested weekly for clasping and grip
147 strength from the age of 7 weeks and until they were 22 weeks old. Body weight was monitored weekly.
148 Clasping was tested by holding the mouse by its tail and lifting it from the top of its home-cage for 10
149 successive trials of three seconds, with three-second rest intervals. The testing was recorded on video,
150 and later scored to evaluate the disease progression. Each three-second trial was scored as following: A)
151 0 points: Normal righting response/no certain abnormalities. Slight collapse of the hind limbs toward the
152 midline was not scored as abnormal unless the hind limbs were at least parallel. Struggling to grab hind
153 limbs or tail with forelimbs was not scored as abnormal. B) 1 point: One hind limb with abnormal
154 retraction or clearly abnormal posture, or both hind limbs abnormally collapsing toward midline until they
155 were at least parallel but without touching or crossing. C) 2 points: Both hind limbs clasping (touching or
156 crossing) after a delay of more than one second or intermittently. D) 3 points: Almost immediate (within
157 the first second) and persistent clasping of hind limbs. The scores from each of the 10 three second trials
158 were summed to give a score from 0-30. Grip strength was tested by letting the mouse grip a horizontal

159 metal bar connected to a newton meter and pulling the mouse away horizontally by the tail. The force
160 recorded by the newton meter was stored digitally by MATLAB software. Grip strength was recorded as
161 the highest value of 10 successive trials. For rotarod testing, open field testing and gait analysis, mice were
162 brought to the testing room in their home-cage for at least one hour before the testing started. All
163 equipment was wiped thoroughly with ethanol between the testing of individual mice. *Rotarod testing:*
164 Rotarod Model LE 8200, Panlab. The male mice were 12 weeks old. Rotation speed accelerated gradually
165 from 4 to 40 rpm over a 5 min period. The mice received four trials per day for three consecutive days for
166 a total of 12 trials with no prior training, and the latency to fall was recorded for each trial. Each mouse
167 only had one attempt to stay on the rotarod for each of the 12 trials. The mice rested in their home-cage
168 for one hour between each trial. *Open field test:* Male mice were tested in the open field and with gait
169 analysis when they were 22 weeks old. Mice were placed in the corner of an open field 40 cm x 40 cm x
170 35cm Plexiglas arena, and the total distance traveled during a 20 min period were recorded automatically
171 using ANY-maze tracking software. *Gait analysis:* Gait analysis was performed in a homemade catwalk
172 apparatus built by our lab. The mice walked through a 50 cm x 5.5 cm corridor with transparent Plexiglas
173 floor to a box on the side of the apparatus containing bedding from their home cage. Green light was lit
174 horizontally through the Plexiglas floor. Ambient red light was used to enhance contrast to the green light
175 reflected down when the mouse placed a paw on the floor. In this way, the paw placement during walking
176 could be accurately determined from a video recorded with the camera of an iPhone SE placed in a fixed
177 holder under the catwalk. A custom-made MATLAB program allowed automatic calculation of stride
178 length for each paw (distance from one placement of the paw to the next placement of the same paw)
179 and the base with of the gait (perpendicular distance from an automatically calculated longitudinal axis
180 of the mouse to the center of the paw). Weekly testing of clasping and grip strength was performed in the
181 room in the animal facility where the mice were normally kept.
182

183 **Electrophysiological experiments**

184 Male mice (P35-45) of indicated genotypes were deeply anesthetized with 4% isoflurane and decapitated.
185 The brain was quickly extracted, transferred to ice-cold artificial cerebral spinal fluid (aCSF) bubbled with
186 95% O_2 and 5% CO_2 and cut into 400 µm coronal slices on a vibratome (Vibratome 3000 Sectioning
187 System). *Recording CA1 of hippocampus:* described in [33]. *Recording dorsal striatum:* Slices containing
188 striatum rostral to and including the level of the commisura anterior were transferred to a grid in a storage
189 chamber with aCSF bubbled with 95% O_2 and 5% CO_2, where they were allowed to recover for at least 1.5
190 hour at RT. The aCSF used for slicing and in the storage chamber contained 126 mM NaCl, 2.5 mM KCl,
191 1.25 mM NaH_2PO_4, 26 mM $NaHCO_3$, 2.5 mM $CaCl_2$, 1.3 mM $MgCl_2$ and 10 mM D-glucose. Slices were then
192 transferred to an interphase recording chamber perfused with aCSF bubbled with 95% O_2 and 5% CO_2 and
193 containing 126 mM NaCl, 2.5 mM KCl, 1.25 mM NaH_2PO_4, 26 mM $NaHCO_3$, 2.0 mM $CaCl_2$, 1.0 mM $MgCl_2$,
194 10 mM D-glucose and 50 µM picrotoxin (Sigma Aldrich) to block $GABA_A$ receptors at a rate of 25 ml per
195 minute. Temperature was kept at stable 31˚C. Field potentials were recorded in current clamp mode using
196 a Multiclamp 700B amplifier (Molecular Devices, Sunnyvale, CA, USA) and a glass microelectrode (7-14
197 MΩ) pulled on a DMZ-Universal puller (Zeitz-Instrumente, Münich Germany) filled with the same aCSF as
198 the interphase chamber. Field excitatory postsynaptic potentials (fEPSPs) were evoked by stimulating
199 white matter in the lower part of the corpus callosum just overlying the dorsomedial striatum with a
200 tungsten concentric bipolar (FHC, Bowdoinham, ME, USA) electrode with pulses of 0.1 ms duration every
201 15 seconds before and after LTP induction. Stimulation intensity was adjusted to evoke fEPSPs at 40-50%
202 of the maximum response on the input-output curve. 10 ng/ml BDNF (Millipore) was added to the aCSF
203 for BDNF rescue experiments. To prevent sequestration of BDNF by unspecific binding to tube surfaces or
204 other surfaces, albumin (0.25%) was also added to the aCSF in BDNF rescue experiments. Picrotoxin (and
205 BDNF) was washed in for at least 20 min before starting the recording of responses. For induction of LTP
206 we employed a theta burst stimulation (TBS) protocol adapted from [40] consisting of 10 trains spaced 15

207 seconds apart. Each train contained 10 bursts of four stimuli with an intraburst frequency of 50 Hz and an
208 interburst theta frequency of 10 Hz. During the TBS protocol stimulation duration was set to 0.3 ms. LTP
209 was induced once baseline had been stable for at least 20 min. Input-output curves were recorded by
210 increasing stimulation intensity from 5% to 30% of 1 mA in 5% increments in the same aCSF as for LTP
211 recordings, including 50 µM picrotoxin. To relieve the magnesium block of NMDA-Rs, all recordings of
212 NMDA-R potentials were done in aCSF containing 0.1 mM $MgCl_2$, 126 mM NaCl, 2.5 mM KCl, 1.25 mM
213 NaH_2PO_4, 26 mM $NaHCO_3$, 2.5 mM $CaCl_2$ and 10 mM D-glucose without picrotoxin. Stimulation intensity
214 during recording of NMDA-R potentials was fixed at 40% of 1 mA for all recordings. When the fEPSPs had
215 been stable for at least 10 min DNQX (Sigma Aldrich), (10 µM) was washed in to block AMPA-Rs. Once the
216 isolated NMDA-R mediated fEPSP had been stable for at least 10 min, RO-25-6981455 (Sigma) (5 µM) and
217 PEAQX (Sigma Aldrich) (0.4 µM) was washed in to further block GluN2B- and GluN2A-containing NMDA-
218 Rs, respectively. fEPSPs were analysed in clampfit 10 (Molecular devices) and the strength of the synaptic
219 potential was quantified as the slope of the fEPSP. LTP was calculated as percent increase of the slope of
220 the fEPSP compared to the average slope of the 20 min baseline. Each point on the LTP summary graphs
221 represent the average of eight consecutive responses. E-LTP at 30 min after LTP induction was calculated
222 as the average of the 10 minutes from 25 min to 35 min after induction of LTP for each recording. L-LTP
223 was calculated as the average of the last 10 minutes of each recording. For analysis of experiments
224 measuring NMDA-R potentials, the combined AMPA-R/NMDA-R response was quantified as the slope of
225 the fEPSP as this best reflected the fast AMPA-R mediated component of the response. The slow NMDA-
226 R component was quantified as the amplitude of the isolated NMDA-R mediated potential.
227

228 **BDNF stimulation of dorsal striatum in acute brain slices from P5 pups**

229 P5 pups were decapitated, the brain quickly extracted and transferred to ice-cold aCSF containing 126mM
230 NaCl, 2.5 mM KCl, 1.25 mM NaH_2PO_4, 26 mM $NaHCO_3$, 2.5 mM $CaCl_2$, 1.3 mM $MgCl_2$ and 10 mM D-glucose

231 bubbled with 95% O_2 and 5% CO_2 and cut into 400 µm coronal slices on a vibratome (Vibratome 3000
232 sectioning system). Slices containing the striatum rostral to and including the level of the commisurra
233 anterior were transferred to a grid in a storage chamber with aCSF bubbled with 95% O_2 and 5% CO_2 where
234 they were allowed to recover for at least 1.5 hour at RT. Thereafter the dorsal striatum was dissected
235 from individual slices while they were still in oxygenated and carbonated aCSF under a stereo microscope.
236 The dorsal striatum from matching hemi-slices was then directly transferred to aCSF continuously bubbled
237 with 95% O_2 and 5% CO_2 containing either 50 ng BDNF/ml or no BDNF for 60 min at 37˚ C with hemi-slices
238 from individual pups (typically three per pup) kept separated in cell strainers. Thereafter, the samples
239 were immediately processed for the subsequent analysis.

240 **Perfusion, fixation, and cryosectioning of brain tissue**

241 To perform transcardial perfusion, the mice were deeply sedated by inhaling 4% isofluorane. Per mouse,
242 we first injected 40ml of ice-cold phosphate buffered saline (1xPBS, pH7.4) to the circulation system to
243 remove all the blood cells. Then we perfused the mice with 40ml of ice-cold 4% formaldehyde (in 1xPBS,
244 pH7.4) to crosslink the tissue. We removed the brain from the skull, and post-fixated it in 4%
245 formaldehyde at +4°C for 24 hours. The next day we washed the brains four times with 1xPBS to remove
246 the leftover formaldehyde, and then we dehydrated the brains in 30% sucrose (dissolved in 1xPBS) at +4°C
247 until the tissue sank down. We then embedded the tissue in OCT cryopreservative and froze it to -80°C.
248 We sectioned 14 µm thick coronal sections containing the dorsal striatum on cryostat Cryostar NX70
249 (Thermo Scientific), which were collected on superfrost plus slides (Thermo Scientific), and stored at -80°C
250 until further use. All procedures were done in parallel for WT and SorCS2 KO mice.

251 **RNA *in situ* hybridization, immunofluorescence, and confocal microscopy**

252 RNA *in situ* hybridization data were obtained from © 2004 Allen Institute for Brain Science. Allen Mouse
253 Brain Atlas Available from mouse.brain-map.org/gene/show/57520. Prior the immunofluorescence, the

254 tissue sections were thaw at room temperature for 30 min, then washed in 1xPBS (pH7.4), gently shaking
255 for 5 min. All stainings were done in parallel for WT and SorCS2 KO sections. We performed antigen
256 retrieval treatment using 1x target retrieval solution (DAKO, #S1699). We first preheated the solution at
257 96°C for 20 min in a FS3000 steamer (Braun), and only then, we added the slides, which were incubated
258 at 96°C for 15min. The sections were transferred into 1xPBS (pH7.4) and washed three times in 1xPBS
259 (pH7.4), gently shaking for 5 minutes. Afterwards, the sections were blocked in PBTA solution (0.1% BSA,
260 0.3% TritonX-100 in PBS, pH7.4) containing 5% donkey serum at room temperature for 1h. The sections
261 were incubated with primary antibodies (diluted in PBTA-5% donkey serum) in a wet chamber overnight.
262 We used following primary antibodies and dilutions: anti-murine-SorCS2 1:100 (#AF4237, R&D Systems),
263 anti-DARPP-32 1:100 (#AB40801, Abcam), anti-NeuN 1:100 (#MAB377, Millipore), anti-GFAP 1:500
264 (#Z0334, DAKO), anti-parvalbumin 1:500 (#AB11427, Abcam), Anti-calretinin 1:500 (#AB5054, Merck
265 Millipore), anti-NPY 1:100 (#11976, Cell Signaling Technology), anti-ChAT 1:100 (#ab70219, Abcam). The
266 next day, the sections were washed 4 times x 5min in 1xPBS (pH7.4) at room temperature, gently shaking.
267 Sections were then incubated with the secondary antibodies (1:800) in PBTA-5% donkey serum for 1.5h
268 at room temperature. We also added Hoechst 1:2000 to stain nuclei. We used AlexaFluor-488 and
269 AlexaFluor-568 conjugated secondary antibodies (Molecular Probes, Invitrogen) of suitable species
270 reactivity. Labelled sections were mounted in Fluorescence Mounting Medium (#S3023, DAKO) and
271 covered by long coverslips. Dorsal striatum was imaged with Zeiss LSM780 or LSM800 confocal
272 microscopes using 10X/0.45, and 40x or 63x/1.20 objectives. We first adjusted the settings to the SorCS2
273 KO tissue and then we applied the same settings for the WT. Acquired images were post-processed in
274 Adobe Photoshop and Adobe Illustrator.

275 **Proximity Ligation Assay (PLA) and super-resolution microscopy**

276 The hemi-slices were handled as free-floating sections. First, they were fixed in 4% formaldehyde for 1
277 hour, washed 3 times with 1xPBS pH7.4 containing 0.1% TritonX-100. Then they were blocked in PBTA

278 solution (described above) for 1 hour in room temperature. For the GluN2B-PSD95 immunofluorescence
279 staining, these primary antibodies were used: anti-GluN2B (1:200, #ab65875, Abcam) and anti-PSD95
280 (1:200, #ab2723, Abcam). The slices were incubated with primary antibodies overnight at +4C. Next day,
281 the slices were washed 3 times with 1xPBS pH7.4 containing 0.1% TritonX-100. We then incubated the
282 slices in secondary donkey antibodies conjugated to AlexaFluor488 and AlexaFluor568 (Molecular Probes,
283 Invitrogen) for 2 hours at room temperature. After that, the slices were washed 3 times with 1xPBS pH7.4
284 containing 0.1% TritonX-100. Then they were placed on Superfrost plus slides (Thermo Scientific),
285 mounted with Fluorescence Mounting Medium (#S3023, DAKO) and covered by long glass coverslips. For
286 the Sorcs2-GluN2B (PLA) + PSD95 (immunofluorescence) staining, the hemi-slices were blocked as
287 described above and incubated with primary antibodies anti-GluN2B (1:200, #ab65875, Abcam), anti-
288 PSD95 (1:200, #ab2723, Abcam), and anti-murine-SorCS2 (1:250, #AF4237, R&D Systems) at 4°C
289 overnight. The next day, the slices were washed 3 times with 1xPBS pH7.4 containing 0.1% TritonX-100.
290 Then we performed the Duolink Fluorescent PLA protocol using Duolink Prober Maker Kit (DUO96010,
291 Sigma Aldrich) as recommended by the manufacturer. We used anti-goat plus (DUO92003, Sigma Aldrich)
292 and anti-rabbit minus (DUO92005, Sigma Aldrich) Duolink PLA probes for the detection of the GluN2B-
293 SorCS2 in close proximity. Secondary donkey anti-mouse antibodies conjugated to AlexaFluor488 (for the
294 detection of PSD95) were applied for 2 hours at room temperature in combination with the far-red
295 detection PLA staining according to the manufacturer protocol. Dorsal striatum was imaged with Zeiss
296 LSM800 confocal microscope using the Airyscan mode for the super-resolution imaging, x63 objective,
297 and voxel size 40x200nm. Co-localization of GluN2B to PSD95 was quantified with the FIJI software as the
298 object area positive for both GluN2B and PSD95 divided by the total object area positive for GluN2B. Co-
299 localization of PSD95 to the SorCS2-GluN2B PLA signal was quantified with the FIJI software as the object
300 area positive for both the PLA and PSD95 divided by the total object area positive for PSD95. All intensity
301 thresholds were obtained with the Fiji autothreshold command. All pixels of the GluN2B-, PLA- and PSD95-

302 positive objects were quantified via the AnalyzeParticles Fiji command. The 3D reconstruction was
303 performed by Imaris 8.2 software.

304 **Tissue dissection and protein extraction**

305 Mice were sacrificed by cervical dislocation. The brain was quickly removed, and transferred to ice-cold
306 1xPBS, pH7.4. The dorsal striatum (upper two thirds of the striatum) rostral to and including the
307 commisurra anterior, and the overlying cortex was dissected out in 1xPBS, pH7.4. The tissue was
308 immediately frozen on dry ice and stored at – 80°C. For western blots, the tissue was homogenized in ice-
309 cold lysis buffer (10mM Tris-base, 150mM NaCl, 1mM EDTA, 1% NP40, pH8) containing freshly added 1x
310 proteases inhibitors (#88666, Thermo Scientific) and 1x phosphatases inhibitors (#4906837001, Roche).
311 In case of stimulated striatal hemi-slices, we immediately homogenised them in separate tubes containing
312 200 uL ice cold lysis buffer (10mM Tris-base, 150mM NaCl, 1mM EDTA, 1% NP40, pH8) containing freshly
313 added 2x proteases inhibitors (#88666, Thermo Scientific) and 2x phosphatases inhibitors (#4906837001,
314 Roche), and 4.5 nM sodium ortovanadate. Samples were centrifuged at 1412g at +4°C for 15 min before
315 the supernatant was transferred to a new tube and kept at - 80˚ C until further analysis.

316 **Real time quantitative PCR (qPCR)**

317 RNA was purified using the Nucleospin gel and PCR clean-up kit from Macherey-Nagel. Complementary
318 DNA (cDNA) was synthetized by using High-Capacity RNA-to-cDNA Kit (#4387406, Applied Biosystems)
319 according to the manufacturer's protocol. For qPCR reaction, TaqMan Fast Advanced Master Mix
320 (#4444556, Applied Biosystems) and TaqMan probes (GAPDH Mm99999915_g1, SorCS2
321 Mm00473050_m1; Thermo Fisher Scientific) were used according to manufacturer´s instructions. The
322 reaction was performed in QuantStudio 7 Flex Real-Time PCR System (Applied Biosystems) using the
323 following program: an activation step at 95°C for 20s, followed by 40 cycles of denaturation at 95°C for 1s

324 and annealing at 60°C for 20s. Next, ΔCp values for each of the samples were calculated by using GAPDH
325 as the reference gene.

326 **ELISA**

327 *BDNF ELISA:* Dorsal striatum and overlying cortex was dissected from 22-week-old mice. The tissue was
328 lysed in ice-cold lysis buffer (10 mM Tris pH 7.4, 150 mM NaCl, 2 mM EDTA, 1% NP- 40, 1% SDS, 1 mM
329 PMSF, 1 µg/ml Aprotinin, 2 µg/ml Leueptine, 1 mM Vanadate, 10 mM NaF and 20 mM β-
330 glycerophosphate) and centrifuged at 14.000 x g for 15 min. For each sample BDNF concentration
331 detected by ELISA was normalized to total protein in the lysate determined by the Bradford method.
332 Detailed protocol is described in [41]. *TrkB-SorCS2 ELISA:* Hippocampal primary cell culture was prepared
333 as described previously [42] from E18 rat embryos. The cells were seeded on 24-well plate and kept in the
334 culture for DIV8-10. Following the treatment with BDNF, cells were lysed for 30min shaking in NP lysis
335 buffer (3M Tris-HCl pH8, 5M NaCl, 0.5M NaF, 1% NP40, 10% glycerol). The ELISA was performed according
336 to the published protocol [43] using these antibodies: anti-TrkB goat 1:1000 (#AF1494, R&D systems),
337 anti-SorCS2 rabbit 1:2000 (#bs-11963R BIOSS), anti-Rabbit IgG HRP-conjugated antibody 1:5000 (#170-
338 5046 BioRad). First, 96-well plate (OptiPlate 96, Perkin Elmer) was coated with anti-TrkB antibody (1:1000
339 in carbonate buffer pH9.8) at +4°C overnight. Then we blocked the plate with 2% BSA in 1xPBS pH7.4 with
340 0.1% Tween20 for 2h at RT, shaking. Afterwards, we added the lysates (120ug of total protein, 100ul/well),
341 sealed the plate, and incubated on a shaker overnight at +4°C. Next, we washed the plate 3 times with
342 1xPBS pH7.4 with 0.1% Tween20, and added anti-SorCS2 antibody (1:2000 in 2% BSA in 1xPBS pH7.4 with
343 0.1% Tween20). We sealed the plate and incubated it on a shaker for 2h at RT or at +4°C overnight. On
344 the third day we washed the plate 3 times with 1xPBS pH7.4 with 0.1% Tween20 and added anti-rabbit
345 IgG HRP-conjugated antibody (RRID:AB_11125757, 100ul/well). We sealed the plate and incubated it on
346 a shaker at RT for 2h. In the end, we washed the plate 3 times with 1xPBS pH7.4 with 0.1% Tween20, and
347 developed the luminescence using premixed ECL reagent (1:1, Pierce, 100ul/well).

348 **Co-immunoprecipitation, Synaptosome extraction, and Western blotting**

349 *Co-immunoprecipitation:* GammaBind G Sepharose beads (50ul/sample; #17-0885-01, GE Healthcare)
350 were washed in 1xPBS (pH7.4) and coated with 1ug of anti-TrkB antibody (#AF1496, R&D Systems) or 1ug
351 of normal Rabbit IgG (#AB-105-C, R&D Systems) while rotating in 1xPBS (pH7.4) ON at 4˚C. The beads
352 were then washed 3 times in 1xPBS (pH7.4), and incubated with 500ul of the lysates of dorsal striatum
353 while rotating at +4°C overnight. The next day, the beads were washed 5 times in 1xPBS-pH7.4 containing
354 0.05% Tween-20. SDS sample buffer (#NP0007, Thermo Fisher Scientific) and 20mM DTT was then added
355 to the washed beads, proteins were denatured by heating to 95°C for 5 min and subjected the SDS-page.
356 *Synaptosome preparation:* For the preparation of synaptosome fraction, we used Syn-PER synaptic
357 protein extraction reagent (#87793, Thermo Scientific). For the extraction, we followed the protocol
358 provided by the manufacturer. In the end of the extraction, we added 1ml of the Syn-PER reagent per 1g
359 of tissue. We resuspended the pellets and measure the protein concentration. We loaded 30ug of protein
360 per well into gradient 4-12% NuPAGE Bis-Tris acryl amid gels (#NP0321, Thermo Fisher Scientific) and
361 performed western blotting analysis.*Western blotting:* Protein concentration of lysates was determined
362 with Bicinchoninic Acid Kit (#BCA1, Sigma Aldrich). Equal amount of proteins was loaded on the poly-
363 acrylamide gels, separated by SDS-page, and transferred to a PVDF membrane by Western blotting in 25
364 mM Tris-base and 192 mM glycine (pH 8.0). Membranes were blocked in 50 mM Tris-base, 0.5 M NaCl,
365 2% skimmed milk powder and 2.1% Tween-20. After blocking membranes were washed for 2 x 5 min in
366 washing buffer containing; 10 mM HEPES, 140 mM NaCl, 2 mM $CaCl_2$, 1 mM $MgCl_2$, 0.2% skimmed milk
367 powder and 0.05% Tween-20 (pH 7.8). Membranes were then incubated with primary antibodies diluted
368 in washing buffer ON at 4˚C. Next day membranes were washed for 3 x 5 min and incubated with HRP-
369 coupled secondary antibodies (DAKO) diluted 1:3000 in washing buffer for 1.5 hour at RT. After washing
370 again for 5 x 5 min western blots were visualized with ECL plus Western Blotting detection system
371 (#RPN2231, GE Healthcare) or Immobilon Forte Western HRP substrate (#WBLUF, Sigma Aldrich)

372 dependent on the signal. We developed the membranes on developing machine LAS4000 (Fuji film). We
373 used following primary antibodies and dilutions: anti-(murine)SorCS2 1:1000 (#AF4237, R&D Systems),
374 anti-DARPP-32 1:1000 (#AB40801, Abcam), anti-BDNF (#P23560, Icosagen), anti-TrkB 1:1000 (#AF1494,
375 R&D Systems), anti-phospho TrkA (Tyr674/675)/TrkB (Tyr706/707) (C50F3) 1:1000 (#4621, Cell signalling
376 technology), anti-GluN1 1:1000 (#5704, Cell signalling technology), anti-GluN2A 1:1000 (#4205, Cell
377 signalling technology), anti-GluN2B 1:1000 (#06-600, Sigma Aldrich), anti-PSD95 1:1000 (#3450, Cell
378 signalling technology), anti-Synaptophysin 1:1000 (#5461T, Cell signalling technology), anti-ERK1/2 1:2000
379 (#4695, Cell signalling technology), anti-pERK1/2 1:1000 (#4370, Cell signalling technology), anti-pAkt
380 1:2000 (#4060, Cell signalling technology), anti-beta-Actin 1:5000 (#A5441, Sigma). The immunoblots
381 were quantified by densitometry in Multigage V3.0 software (Fuji film) or ImageJ software. We
382 substracted background and normalized the signal to loading control. For BDNF stimulation assay, we
383 normalized phosphorylated TrkB to total levels of TrkB.

384 **Statistics**

385 We used GraphPad Prism 9.1.2 for the data visualization and statistical analysis. All data sets were
386 evaluated for normality and statistical outliers. The data are presented as mean ±SEM. For simplicity, the
387 symbols * indicate $p<0.05$, ** indicate $p<0.01$, *** indicate $p<0.001$, and **** indicate $p<0.0001$. An
388 overview of used statistical tests can be found in the **Table 1**.

389

390 # RESULTS

391 ## SorCS2 is selectively expressed by MSNs in dorsal striatum

392 SorCS2 is typically expressed by neurons in the adult mouse brain, with the highest expression in dentate
393 gyrus of the hippocampus and piriform cortex [33, 44]. To explore SorCS2 expression profile in

394 corticostriatal circuits, we first took advantage of the available *in situ* hybridization data (IHC) from Allen
395 brain atlas. We observed that besides the piriform cortex, SorCS2 is highly expressed in dorsal striatum
396 (caudoputamen), cortical layers II and III (including motor cortex and anterior cingulate cortex), induseum
397 griseum, and intermediate lateral septal nucleus (**Figure 1a-c)**. To determine which cell types express
398 SorCS2 in dorsal striatum, we performed immunofluorescence using a number of known cell type-specific
399 markers. Age-matched SorCS2 knockout (KO) brain tissue served as negative control. We found that
400 SorCS2 is expressed by DARPP-32 and NeuN positive neurons (**Figure 1d-e**) that designates MSNs in dorsal
401 striatum. On contrary, SorCS2 was absent from any of the most prominent types of striatal interneurons
402 [45, 46] such as calretinin positive interneurons, large aspiny cholinergic interneurons (ChaT+), GABAergic
403 fast-spiking parvalbumine-positive interneurons, and low-threshold-spiking neuropeptide Y (NPY+)
404 interneurons (**Suppl. Figure S1a-d**). As previously reported for the hippocampus, SorCS2 was absent in
405 Glial fibrillary acidic protein positive (GFAP+) glia cells in dorsal striatum (**Suppl. Figure S2**). Our data
406 suggest that SorCS2 may be involved in the biology of MSNs in the dorsal striatum.
407

408 ## SorCS2 deficiency accelerates HD progression in R6/1 mice

409 Since MSNs in dorsal striatum control motor skills, we studied motor function in SorCS2 KO and tested
410 whether SorCS2 deficiency worsens HD-related motor symptoms. To address this, we generated double
411 transgenic line by crossing SorCS2 KO mice into the R6/1 transgenic HD model, which carries a human 115
412 CAG repeat in exon 1. First, we subjected 12 weeks old males to rotarod behavior testing to study motor
413 skill learning. Mice were placed on the accelerating rotarod without any prior training and received four
414 trials per day for three consecutive days. Each mouse had a single attempt on the rotarod for each trial
415 and we recorded the latency to fall (**Figure 2a**). This experiment revealed a significant role of genotype
416 ($p=0.014$) and trial number ($p=<0.0001$) in motor performance. SorCS2 KO mice and R6/1 mice both
417 displayed impaired motor skill learning, as did the double transgenic SorCS2 KO; R6/1 mice [SorCS2 KO vs

418 WT (p=0.0006), R6/1 vs WT (p=<0.0001), SorCS2 KO; R6/1 vs WT (p=0.0002), SorCS2 KO vs R6/1
419 (p=0.0154)]. At this age, there was no additive effect of SorCS2 loss of function to motor learning and HD
420 progression in the R6/1 line.
421
422 To study the progression of HD, we next monitored the mice from 7 weeks to 22 weeks of age with respect
423 to body weight, grip strength, and clasping. Both, SorCS2 KO and R6/1 males had lower body weight than
424 WT (p<0.0001 and p=0.0006, respectively), which was further reduced in SorCS2 KO; R6/1 mice when
425 compared to R6/1 (p=<0.0001) and SorCS2 KO (p=0.0028) (**Figure 2b**). The same applied to females
426 [SorCS2 KO vs WT (p=<0.0001), R6/1 vs WT (p=<0.0001), SorCS2 KO; R6/1 vs R6/1 (p=<0.0001)] (**Suppl.**
427 **Figure S3a**). Grip strength was tested by letting the mouse grip a horizontal metal bar connected to a
428 newton meter, and pulling the mouse away horizontally by the tail. Grip strength was diminished in R6/1
429 mice in both males (p=<0.0001) (**Figure 2c**) and females (p=0.0009) (**Suppl. Figure S3b**). However, SorCS2
430 KO mice did not stand out from WT, and neither did receptor deficiency aggravate the phenotype of R6/1
431 in this paradigm. We next tested for clasping, which is a marker of neurodegeneration commonly used to
432 study disease progression in HD mice [38]. The mice may initially present a dystonic posture that, as the
433 disease builds up, eventually develops into overt clasping of the hind limbs when lifted by the tail. SorCS2
434 KO displayed minor clasping when compared to WT in both males (p=0.0059) (**Figure 2d**) and females
435 (p<0.0001) (**Suppl. Figure S3c**). As expected, R6/1 mice exhibited significant clasping [(p<0.0001), both
436 genders]. Strikingly, we observed a severe worsening of clasping in SorCS2 KO; R6/1 mice when compared
437 to R6/1 [(p<0.0001) both genders], which accelerated with aging (males: p=0.0118, females: p<0.0001).
438 This observation manifested an important contribution of SorCS2 loss of function on HD progression.
439
440 To assess gait performance, we recorded the movement of 22 weeks old males using an in-house-built
441 catwalk apparatus. The assay enabled us to distinguish single steps of a walking mouse, and measure the

442 stride length and the base width of the gait (**Figure 2e, Suppl. Figure S3d**). Representative videos for WT,
443 SorCS2 KO, R6/1, and SorCS2 KO; R6/1, respectively, are available in **Suppl. Video SV1-4**). The double
444 transgenic line showed impaired gait pattern through the corridor (**Figure 2e, Suppl. Figure S3e**). Image
445 analysis revealed that SorCS2KO; R6/1 mice have significantly reduced front limb stride length compared
446 to the R6/1 (p=0.0043), while the single transgenic lines performed as WT (**Figure 2f**). Hind limb stride
447 length was also significantly reduced in SorCS2 KO; R6/1 mice compared to R6/1 mice (p=0.0038) (**Figure**
448 **2g**), and hind limb base width was increased only in SorCS2KO; R6/1 compared to the other genotypes; to
449 WT (p=0.0009), SorCS2 KO (p=0.0141), and R6/1 (p=0.0133) (**Figure 2h**). These data indicate that the
450 impaired gait performance is caused by cumulative effect of SorCS2 loss of function in the HD model.
451 Finally, we subjected 22 weeks old males to the open field test. In this test, R6/1 as well as SorCS2KO;
452 R6/1 mice moved less than WT (p=0.0061 and p<0.0001, respectively) and with significant worsening of
453 the activity in SorCS2 KO; R6/1 compared to the R6/1 mice (p=0.0082) (**Figure 2i**). Taken together, our
454 data demonstrate that SorCS2 loss of function accelerates and worsens some of the HD-related motor
455 symptoms in R6/1 mice.
456

457 ## Striatal expression of SorCS2 and DARPP-32 during HD progression

458 To investigate whether HD progression affects SorCS2 expression, we examined RNA and protein levels in
459 our transgenic mice using the real-time quantitative PCR (qPCR) and western blot analyses. While SorCS2
460 expression in the dorsal striatum of 6 weeks old asymptomatic R6/1 mice did not differ from WT mice
461 (**Suppl. Figure S4a-b**), it was reduced by 50% both at protein (p=0.0001) and RNA levels (p=0.0019) in 22
462 weeks old symptomatic animals (**Figure 3a-c**). This difference was tissue specific as SorCS2 expression in
463 cortex was unaltered (**Suppl. Figure S4d-f**). Hence, a reduction of striatal SorCS2 expression may
464 accelerate and exacerbate the HD progression. A decline in DARPP-32 is known to reflect the
465 neurodegenerative process of MSNs in several HD mouse models [23, 47]. We found that DARPP-32

466 expression in 6 weeks old asymptomatic R6/1 mice was normal (**Suppl. Figure S4a, c**). However, at 22
467 weeks of age, DARPP-32 was significantly reduced in both R6/1 (p=0.0082) and SorCS2 KO; R6/1 mice
468 (p=0.0044). DARPP-32 was unaltered in *Sorcs2*$^{-/-}$ mice of similar age (**Figure 3d, 3g**). The data suggest that
469 a secondary reduction in SorCS2 expression may fuel the HD progression, possibly by altering MSNs
470 function rather than by directly affecting their degeneration.

471 SorCS2 is required for robust TrkB signaling in dorsal striatum

472 Reduced BDNF signaling is fundamental to the neurodegenerative process and altered neurotransmission
473 of MSNs. In some HD mouse models, the cortical transcription of BDNF, its anterograde transport and
474 release from cortical terminals in the dorsal striatum, as well as the TrkB expression are suppressed [6, 7,
475 12, 13, 23, 48]. In other cases, BDNF and TrkB expression is preserved but TrkB signaling is compromised
476 [8, 28, 41]. We therefore quantified BDNF and TrkB levels in corticostriatal circuits to study the impact of
477 SorCS2 on TrkB signaling. Despite severe motor symptoms in the R6/1 and SorCS2 KO; R6/1 mice, BDNF
478 levels were not reduced in cortex nor in dorsal striatum, indicating that the production and trafficking of
479 BDNF is unaffected by mHTT and SorCS2 (**Suppl. Figure S4g-j**). However, we observed an increase in BDNF
480 levels in dorsal striatum of SorCS2 KO; R6/1 when compared to SorCS2 KO (**Suppl. Figure S4h)** which might
481 indicate a compensation in BDNF secretion to overcome the neurodegeneration. There was also no
482 difference in BDNF maturation, as we observed no shifts in the ratio between proBDNF and BDNF levels
483 in dorsal striatum (**Suppl. Figure S4i-j**). Expression of the full-length TrkB receptor was slightly increased
484 in the SorCS2 KO mice (p=0.0482) but this difference disappeared on the R6/1 background (**Figure 3d-e**).
485 The expression of the truncated TrkB variant (named TrkB-T.1) was independent of genotype (**Figure 3d,
486 f**). We next investigated whether SorCS2 may physically interact with TrkB to control its signalling abilities.
487 To this end, TrkB was immunoprecipitated from dorsal striatum and the precipitate probed for SorCS2.
488 Indeed, we found that the two receptors co-immunoprecipitated demonstrating that SorCS2 and TrkB can
489 physically interact to form a heteromeric complex (**Figure 4a**). Strikingly, in primary hippocampal cultures,

490 this interaction was increased by approximately 200% when treated with 10 ng/ml BDNF (**Figure 4b**). We
491 then asked if SorCS2 enables BDNF-TrkB signaling in the histologically intact dorsal striatum. BDNF-
492 induced TrkB phosphorylation in *ex vivo* striatal slices is detectable in newborn pups, peaks around P7,
493 thereafter it declines, and disappears around P12 [49, 50]. Hence, we prepared acute brain slices from P5
494 pups that were maintained in artificial cerebral spinal fluid (aCSF). Dorsal striatum from one set of hemi-
495 slices was stimulated with 50 ng/ml BDNF (in aCSF) for 1 hour, while the other set of matching hemi-slices
496 were incubated only in aCSF serving as unstimulated control. BDNF treatment induced a 2.3-fold increased
497 phosphorylation of TrkB when normalized to total TrkB (p=0.0023) (**Figure 4c-d**). Strikingly, when
498 comparing the response to BDNF treatment in WT and SorCS2 KO mice, we found that TrkB
499 phosphorylation was reduced by 63% in slices from the knockouts (p=0.0047) (**Figures 4d**). We thus
500 conclude that SorCS2 binds TrkB in a BDNF-dependent manner, and that this interaction is required for
501 robust TrkB phosphorylation in the dorsal striatum.
502

503 ## SorCS2 promotes BDNF-dependent LTP in dorsal striatum

504 Given a critical role of BDNF-TrkB signaling in NMDAR-dependent LTP, we investigated if SorCS2 modifies
505 synaptic potentiation in the corticostriatal synapses. We first examined α-amino-3-hydroxy-5-methyl-4-
506 isoxazolepropionic acid receptor (AMPAR) activity by recording input-output (I/O) curves in the dorsal
507 striatum in P35-45 mice. Field potentials were evoked in the white matter by stimulating the lower part
508 of the corpus callosum directly overlying the dorsal striatum, and the synaptic response was quantified as
509 the slope of the field excitatory postsynaptic potential (fEPSP). The I/O curves showed no differences in
510 AMPAR activity between genotypes (**Figure 5a-b**). We then applied a theta burst stimulation (TBS)
511 protocol for induction of LTP [40]. A stable baseline of at least 20 min preceded the TBS, and LTP was
512 subsequently quantified as the percentage increase in the slope of the fEPSP compared to the baseline.
513 Notably, whereas we observed robust LTP in WT slices for up to 180 min post stimulation (p<0.0001), LTP

514 was substantially impaired in both the SorCS2 KO and R6/1 mice ($p<0.0001$ for both conditions) (**Figure**
515 **5c**). To explore whether the perturbed BDNF-TrkB signaling accounted for the blunted LTP in SorCS2 KO
516 and R6/1 mice, we performed rescue experiments in which 10ng/ml BDNF was supplemented to the aCSF
517 (**Figure 5d-g**). In WT mice, LTP was maintained although with reduced amplitude (**Figure 5e)**. This is in
518 accordance with studies reporting that acute exposure to BDNF increases basal synaptic potentiation and
519 reduces LTP in WT mice [51]. Remarkably, BDNF fully restored LTP in SorCS2 KO slices as the synaptic
520 strength was established at the same level as observed for untreated WT sections (**Figure 5f**). Hence, the
521 attenuated BDNF-TrkB signaling in *Sorcs2-/-* mice can be overcome by addition of exogenous BDNF. On
522 the contrary, BDNF failed to rescue the LTP in R6/1 mice. This data suggest that the functional deficits in
523 the R6/1 mice are either a consequence of complete block in TrkB signaling or defects in BDNF-
524 independent pathways (**Figure 5g**). All the measurements and statistics are summarized in (**Figure 5h**).
525

526 ## Synaptic function of GluN2B is controlled by SorCS2

527 Synaptic accumulation and conductance of NMDA receptors is required for the induction of BDNF-
528 dependent LTP [52]. We therefore compared NMDAR currents in the dorsal striatum of 35-45 days old
529 SorCS2 KO and R6/1 mice. The recordings were performed in 0.1 mM magnesium to partially relieve the
530 magnesium block of the NMDARs. Once AMPAR- and NMDAR-mediated potentials were stable, we first
531 blocked AMPARs by adding the antagonist, cyanquixaline (DNQX) (**Figure 6a**). NMDAR potentials were
532 then measured as the amplitude of the slow potential and normalized to the slope of the AMPAR-
533 mediated potentials. We found that synaptic NMDAR-mediated currents were substantially attenuated in
534 both SorCS2 KO and R6/1 mice (corresponding to approximately 60%), followed by a severe worsening of
535 the phenotype (down to 31%) when the lines were crossbred (**Figure 6b**). Next, we explored the relative
536 contribution of GluN2A and GluN2B to the total NMDAR conductivity. To this end, neurotransmission was
537 recorded in brain slices treated with the selective GluN2B inhibitor RO 25-6981 maleate, followed by the

538 GluN2A inhibitor PEAQX, respectively (**Figure 6a**). The GluN2B and GluN2A components were then
539 calculated and normalized to the AMPAR currents for each experiment. Strikingly, we found that the
540 attenuated NMDA currents in *Sorcs2*$^{-/-}$ animals were entirely accounted for by elimination of GluN2B
541 neurotransmission (**Figure 6d)** with no impact on the GluN2A activity (**Figure 6c**). We measured a similar
542 selective regulation in GluN2B activity in hippocampal CA3-CA1 synapses (**Suppl. Figure S5**), suggesting a
543 more general function of SorCS2 in controlling NMDAR dependent neurotransmission. In marked contrast
544 to SorCS2 KO, only GluN2A currents were affected in the dorsal striatum of the R6/1 mice (**Figure 6c-d**).
545 These findings show that SorCS2 deficiency and the accumulation of mHTT affect the synaptic plasticity
546 by different modes of action, which may explain why mice harboring both impairments have a more
547 severe disease course.
548

549 ## SorCS2 targets GluN2B to postsynaptic densities in a BDNF-dependent manner

550 To explore whether the effect of SorCS2 on synaptic plasticity was a consequence of altered expression
551 of GluN2B or other key synaptic proteins, we performed western blotting of homogenates and
552 synaptosomes from the dorsal striatum of WT and SorCS2 KO mice, age P35 (**Suppl. Figure S6a**). In the
553 synaptosome fractions, we found no alterations in the NMDAR subunits GluN1, GluN2A, and GluN2B,
554 neither in synaptophysin and pAkt levels (**Suppl. Figure S6b-d, g, k**). However, PSD95, TrkB, total Erk1/2,
555 and pErk1/2 (but not the ratio between pErk and Erk1/2) were all increased in the homogenates (**Suppl.
556 Figure S6e, f, h-j**), possibly to compensate for the reduced ability of BDNF to activate TrkB (*cf.* **Figure 4c-
557 d**). Total Erk1/2 was increased in synaptosomes, but this did not translate into any alterations in Erk1/2
558 phosphorylation (**Suppl. Figure S6h-j**)**.** Hence, the impaired GluN2B activity of corticostriatal synapses in
559 the SorCS2 KO mice is not accounted for by altered expression of NMDARs or the selected synaptic
560 proteins involved in the neurotransmission.
561

562 BDNF regulates the synaptic targeting and conductance of GluN2B in the corticostriatal pathway [18, 19,
563 53-55]. We therefore studied GluN2B expression in synapses of the dorsal striatum from SorCS2 KO mice
564 with or without prior BDNF stimulation. The sections were immunostained for PSD95 and GluN2B,
565 processed by Airy-scan super-resolution microscopy. Strikingly, GluN2B co-localization with PSD95 was
566 lower by approximately 25% in the unstimulated SorCS2 KO slices compared to WT mice (**Figure 6e-f**).
567 Furthermore, BDNF treatment increased postsynaptic enrichment of GluN2B by approximately 50% in WT
568 mice (from 7.5% to 11.25%) but SorCS2 KO mice were completely refractory. Hence, it is likely that local
569 activation of GluN2B already present at the synapse, rather than its recycling and recruitment from
570 extrasynaptic sites, is accountable for the restoration of LTP by BDNF in SorCS2 deficient mice. These data
571 suggest that SorCS2, aside from its ability to support TrkB signaling, also directly enables the synaptic
572 targeting of GluN2B.

573 Finally, we asked whether SorCS2, similarly to its interaction with TrkB, might physically interact with
574 GluN2B in a BDNF-dependent manner. To this end, we used proximity ligation assay (PLA) for SorCS2 and
575 GluN2B interaction. This method labels proteins that are closely juxtapositioned. Immunofluorescence
576 microscopy revealed that the receptors co-localize throughout MSNs in naïve WT slices. Strikingly,
577 stimulation with BDNF reduced the SorCS2-GluN2B interaction in MSNs by 60% indicating disengagement
578 of the SorCS2-GluN2B complex (**Figure 6g-h**). Remarkably, almost 50% of the SorCS2-GluN2B PLA puncta
579 were present in PSD95-positive domains in the unstimulated dorsal striatum, but BDNF treatment
580 completely abolished the synaptic co-localization (**Figure 6i**). Taken together, the data demonstrate that
581 SorCS2 binds GluN2B to enable its translocation to the synapse, after which BDNF abolishes their
582 heterodimerization. This may stabilize the synaptic expression of the NMDAR subunit and condition it for
583 neurotransmssion.

584 # DISCUSSION

585 In the healthy brain, BDNF-TrkB signaling serves two functions; it enables the activity-dependent
586 regulation of synaptic structures and function, and it supports the neuronal integrity through trophic
587 stimulation. A cornerstone in the HD neuropathology is the diminished BDNF activity as consequence of
588 reduced BDNF production or its impaired anterograde transport from cortex to striatum, or decreased
589 expression or signalling abilities of TrkB. At early stages of the disease, altered NMDA receptor activity
590 caused by reduced BDNF-TrkB signaling is considered fundamental while at later stages lowered
591 neuroprotection may propel the pathophysiological changes [56, 57]. Accordingly, some HD mouse
592 models develop overt neurodegeneration, whereas in other models synaptic disturbances such as
593 disrupted NMDA-dependent LTP manifest but without apparent loss of neurons [8, 28, 58]. Here we
594 identified SorC2 as a molecular hub that regulates BDNF signaling, synaptic plasticity, and HD progression
595 through dynamic changes in its physical interactions with TrkB and GluN2B.

596

597 We show that SorCS2 is selectively expressed by MSNs in dorsal striatum, and that the performance of
598 SorCS2 KO mice on the rotarod is compromised. Most likely, this effect was not accounted for by neuronal
599 cell loss since the surrogate parameters of neuronal degeneration DARPP-32 and clasping were not altered
600 in the aged SorCS2 knockouts. On the other hand, SorCS2 deficiency on the R6/1 genetic background
601 severely aggravated the motor phenotypes and accelerated the disease progression. One of the earliest
602 alterations during HD development is a dysfunction of corticostriatal synapses [56]. In HD mouse models
603 such as BACHD, Q175, or HdhQ7/Q111, the motor deficits have been attributed to the loss of LTP [8, 59].
604 BDNF signalling is fundamental for ionotropic potentiation, and both GluN2A and GluN2B are required for
605 LTP in corticostriatal synapses [8, 60, 61]. In hippocampal neurons, the activation of TrkB results in
606 phosphorylation of GluN1 [62] and GluN2B subunits [18, 19], but not GluN2A [63], which is required for
607 synaptic trafficking of NMDA receptors and LTP induction [53]. We found that SorCS2 binds TrkB in BDNF-

608 dependent manner, and that this interaction is required for efficient activation of TrkB. Furthermore, the
609 absence of SorCS2 caused a significant decrease in TrkB phosphorylation and abolished LTP in the
610 corticostriatal pathway. These features were probably caused by a severe deficiency in GluN2B currents
611 as the neurotransmission by GluN2A was preserved. Our findings contrast those of *Ma et al 2017* who
612 reported that GluN2A expression is decreased in MSNs from SorCS2 KO mice. However, the authors did
613 not study any functional consequences of their observation [64]. Although we cannot discount the
614 possibility that SorCS2 affects the subcellular distribution of GluN2A, it does not seem to be of major
615 functional significance. In contrast to SorCS2 deficient mice, GluN2A currents were affected only in the
616 R6/1 line. This is in accordance with a recent study that reported reduced LTP, impaired GluN2A but
617 unaltered GluN2B activity in the hippocampus of R6/1 mice [65]. In our SorCS2 KO; R6/1 double transgenic
618 mice, GluN2A and GluN2B were both severely attenuated which translated into a marked reduction in
619 total NMDA receptor currents. This observation may explain the worsening of the behavioral phenotypes
620 in our double transgenic mice.
621
622 Aside from the function of SorCS2 in TrkB activation, which induces phosphorylation of GluN2B and GluN1
623 that is necessary for their synaptic enrichment, SorCS2 also modulates GluN2B function through a direct,
624 BDNF-independent interaction. Co-immunoprecipitation experiments recently showed that SorCS2 and
625 GluN2B form heterodimers in hippocampal extracts [66]. We found that synaptic clustering of GluN2B in
626 the dorsal striatum from SorCS2 KO was reduced by 25% compared to WT mice. Furthermore, GluN2B
627 currents in naïve, unstimulated slices were diminished by 80% in SorCS2 KO while GluN2A currents
628 remained unaffected. Strikingly, the interaction between SorCS2 and GluN2B was dynamic in MSNs as
629 BDNF disrupted the complexes. SorCS2 is engaged in several aspects of protein sorting directing its cargo
630 between Golgi, cell surface and endosomes [36]. Notably we previously found that SorCS2 facilitates the
631 synaptic translocation of TrkB to postsynaptic densities in hippocampal neurons [33]. Given its many

632 trafficking pathways, SorCS2 could potentially enable the synaptic insertion of GluN2B during exocytosis,
633 its lateral diffusion between the synapse and extrasynaptic sites, or its endocytosis and recycling. Even
634 though the sorting pathway is currently unclear, our study identifies SorCS2 as a novel sorting mechanism
635 to regulate the postsynaptic membrane localization of GluN2B.
636
637 Psychiatric symptoms are common in HD [1]. Our previous studies discovered that SorCS2 KO mice exhibit
638 cognitive impairments and traits typifying ADHD and schizophrenia [33, 37]. Similarly to the dorsal
639 striatum, ionotropic LTP was absent in CA3-CA1 synapses but could be rescued by exogenous BDNF. Here
640 we find that GluN2B but not GluN2A currents are substantially reduced also in CA3-CA1 synapses,
641 suggesting a broader function of SorCS2 in modifying NMDAR-dependent plasticity. SorCS2 plays an
642 important role for dopaminergic functionality as SorCS2 deficiency severely perturbs dopaminergic firing
643 rates in the ventral tegmental area, striatal dopamine metabolism, and dopamine D1 receptor (D1R)
644 sensitivity [35, 37]. Inquiringly, D1R cooperates with TrkB to modulate ERK signalling in striatal neurons
645 and to increase GluN2B phosphorylation [67, 68]. Given that dysfunctional striatal dopamine signalling
646 contributes to the HD pathophysiology in mouse models [69], it is possible that yet another loop may be
647 added to the many functions of SorCS2 in Huntington's disease.
648
649 SorCS2 mRNA and protein levels were reduced in the dorsal striatum of symptomatic R6/1 mice with no
650 changes in cortex. Interestingly, the expression level was dependent on age and HD progression as it was
651 not detected in young asymptomatic mice. A separate study reported reduced SorCS2 expression also in
652 zQ17Z and R6/2 HD mice [64]. Inversely, others found upregulation of SorCS2 mRNA in MSNs in response
653 to deep-brain stimulation in a Parkinson's disease mouse model [70]. It appears that SorCS2 expression in
654 MSNs is highly controlled by internal and external stimuli, and can dynamically change, e.g. as a reaction
655 to pathophysiological changes in the tissue. A recent study reported that mHTT can bind SorCS2 leading

656 to its redistribution and aggregation in MSNs [64]. Hence, in addition to attenuated gene transcription,
657 scavenging of SorCS2 protein by mHTT may further reduce its expression in MSNs.
658
659 Taken together, we provide evidence that SorCS2 operates by two mechanisms to orchestrate GluN2B-
660 dependent plasticity in MSNs. First, it associates with TrkB to enable its activation by BDNF, which is
661 required to phosphorylate GluN2B and to empower GluN2B enrichment at the postsynaptic densities.
662 However, in parallel to this, SorCS2 may assist in targeting GluN2B to the synapse through their direct
663 interaction. Once at the synapse, BDNF uncouples SorCS2 from GluN2B, which may condition GluN2B for
664 the required biological activity. The dynamic interaction of SorCS2 with TrkB, and GluN2B, respectively,
665 might thus produce an amplifying loop where SorCS2, which is liberated from GluN2B by BDNF, can be
666 reused by TrkB to further fuel BDNF signaling, phosphorylation of GluN2B, and the induction of LTP. This
667 proposed model is schematized in the **Figure 7**. Even though the primary determinant of HD onset is the
668 length of the CAG repeats on the expanded allele [1, 71], yet this only accounts for 50-70% variations in
669 the age of onset [30, 31, 71, 72] . Notably, a recent GWAS study identified SNPs and missense mutations
670 in *SORCS2* associated with HD [32], and another study has reported reduced levels of SorCS2 mRNA in
671 post-mortem brains of HD patients [73]. Here we have provided mechanistic support for *SORCS2* as one
672 of the long-sought disease modifying genes in Huntington's disease.
673

674 # CONCLUSIONS

675 Reduced BDNF-TrkB signaling and NMDAR-dependent synaptic plasticity are hallmarks of early stages of
676 Huntington's disease. We show that SorCS2 enables TrkB activation and navigates GluN2B to MSN
677 synapses. The binding between SorCS2 and TrkB and GluN2B, respectively are mutually exclusive and
678 controlled by BDNF. While BDNF stimulates complex formation between SorCS2 and TrkB to amplify BDNF

679 signaling, it uncouples SorCS2 from GluN2B resulting in enrichment of the neurotransmitter subunit at
680 postsynaptic densities. During HD progression SorCS2 expression declines which compromises BDNF-TrkB
681 signaling and NMDAR-dependent plasticity thereby accelerating the disease course. These findings may
682 nominate SorCS2 as therapeutic target to slow down the progression of Huntington´s disease.
683

684 LIST OF ABBREVIATIONS

685 aCSF – artificial cerebral spinal fluid
686 AMPAR – α-amino-3-hydroxy-5-methyl-4-isoxazolepropionic acid receptor
687 BDNF – Brain-derived neurotrophic factor
688 Cf. – cross reference
689 D1R – dopamine D1 receptor
690 DS – dorsal striatum
691 fEPSP - field excitatory postsynaptic potential
692 GFAP - Glial fibrillary acidic protein
693 GluN1/2B/2A – Glutamate Ionotropic Receptor NMDA Type Subunit 1/2B/2A
694 GWAS – genome-wide association study
695 HD – Huntington's disease
696 HTT/mHTT– Huntingtin / mutated Huntingtin
697 I/O – input-output curves
698 IHC – in situ hybridization
699 IP - immunoprecipitation
700 KO – knock out
701 LTP – long-term potentiation
702 MC – multi comparison test
703 MSNs – medium spiny neurons
704 NMDAR - N-methyl-D-aspartate receptor

705 PLA – proximity ligation assay

706 proBDNF – precursor of Brain-derived neurotrophic factor

707 qPCR – real-time quantitative polymerase chain reaction

708 RBI – relative band intensity

709 SEM – standard error of mean

710 SNP – single nucleotide polymorphism

711 SorCS2 - Sortilin Related VPS10 Domain Containing Receptor 2

712 TBS – theta burst stimulation

713 TrkB – Tropomyosin related kinase receptor B

714 TrkB-FL – full length Tropomyosin related kinase receptor B

715 TrkB-T.1 – Truncated variant of Tropomyosin related kinase receptor B

716 WT – wild type

717

718

719 DECLARATIONS

720 **Ethics approval**

721 Animal experiments were performed in full compliance with Danish and European regulations. All

722 experiments are covered by permissions: 2012-15-2934-00397 (C3) and 2017-15-0201-01192 (C3) issued

723 by the Danish Animal Experiments Inspectorate.

724 **Consent for publication**

725 Not applicable

726 **Availability of data and materials**

727 Not applicable

728 **Competing interests**

729 The authors declare that they have no competing interests.

730 **Funding**

731 This study was supported and funded by the Lundbeck Foundation (R248-2017-431 and DANDRITE-R248-
732 2016-2518), Danish National Research Foundation (DNRF133; PROMEMO – A Center of Excellence for
733 Proteins in Memory), and by the Danish Council for Independent Research (DFF-7016-00261). JCA
734 laboratory was funded by the Spanish government grant (BFU2017-822667) and by the EU 7th Framework
735 Program (PAINCAGE). EC laboratory was supported by Academy of Finland, Jane & Aatos Erkko foundation
736 and Sigrid Juselius foundation.

737 **Authors' contributions**

738 AS performed some experiments, analyzed the data, wrote the manuscript, prepared all the figures, and
739 coordinated finalization of the study; this determined her to become the first shared first-author. NSD
740 planned and conducted some experiments, analyzed the data, and wrote a manuscript draft. MP
741 performed SR microscopy and analyzed the data. MP provided unique insight into the molecular
742 mechanism, and this is why he is the first shared-second author. NKM helped with behavior experiments,
743 built the catwalk assay, and developed MATLAB programs for analyzing behavioral data. PLO helped with
744 synaptosomes preparation and electrophysiological measurements. BV helped with conducting the mice
745 work and performed some biochemical experiments. SLB and JCA measured BDNF and proBDNF levels.
746 PC and EC provided the ELISA data for TrkB-SorCS2 interaction. AU analyzed the synaptic proteins in
747 synaptosomal extraction. LK isolated the synaptosomes and performed some pioneer pulldown
748 experiments. LW performed qPCR. IF and SN helped with *in vivo* experiments that were not included in
749 the final study. MMH provided input and support to the electrophysiological experiments. MFK trained
750 NSD in performing biochemical experiments and drafting the manuscript. UB trained NSD, and performed
751 some electrophysiological experiments. AN designed the study, coordinated the research, and wrote the
752 manuscript.

Acknowledgements

We acknowledge Kristian Skipper Alsberg and Anne Kathrine Aalling Sørensen for their technical involvement in part of the project, which was not included in this manuscript. We thank Sune Skeldal and Anne Kerstine Glintborg Jensen for the technical help, and Stella Solveig Nolte for coordinating the mice work, and for the genotyping. We thank the department of Biomedicine at Aarhus University for providing the infrastructure and administrative support.

REFERENCES

1. Ross CA, Tabrizi SJ: **Huntington's disease: from molecular pathogenesis to clinical treatment.** *The Lancet Neurology* 2011, **10:**83-98.
2. Jimenez-Sanchez M, Licitra F, Underwood BR, Rubinsztein DC: **Huntington's Disease: Mechanisms of Pathogenesis and Therapeutic Strategies.** *Cold Spring Harbor perspectives in medicine* 2017, **7**.
3. Bates GP, Dorsey R, Gusella JF, Hayden MR, Kay C, Leavitt BR, Nance M, Ross CA, Scahill RI, Wetzel R, et al: **Huntington disease.** *Nature reviews Disease primers* 2015, **1:**15005.
4. McColgan P, Tabrizi SJ: **Huntington's disease: a clinical review.** *Eur J Neurol* 2018, **25:**24-34.
5. Zuccato C, Ciammola A, Rigamonti D, Leavitt BR, Goffredo D, Conti L, MacDonald ME, Friedlander RM, Silani V, Hayden MR, et al: **Loss of huntingtin-mediated BDNF gene transcription in Huntington's disease.** *Science (New York, NY)* 2001, **293:**493-498.
6. Gauthier LR, Charrin BC, Borrell-Pagès M, Dompierre JP, Rangone H, Cordelières FP, De Mey J, MacDonald ME, Lessmann V, Humbert S, Saudou F: **Huntingtin controls neurotrophic support and survival of neurons by enhancing BDNF vesicular transport along microtubules.** *Cell* 2004, **118:**127-138.
7. Liot G, Zala D, Pla P, Mottet G, Piel M, Saudou F: **Mutant Huntingtin alters retrograde transport of TrkB receptors in striatal dendrites.** *The Journal of neuroscience : the official journal of the Society for Neuroscience* 2013, **33:**6298-6309.
8. Plotkin JL, Day M, Peterson JD, Xie Z, Kress GJ, Rafalovich I, Kondapalli J, Gertler TS, Flajolet M, Greengard P, et al: **Impaired TrkB receptor signaling underlies corticostriatal dysfunction in Huntington's disease.** *Neuron* 2014, **83:**178-188.
9. Jiang M, Peng Q, Liu X, Jin J, Hou Z, Zhang J, Mori S, Ross CA, Ye K, Duan W: **Small-molecule TrkB receptor agonists improve motor function and extend survival in a mouse model of Huntington's disease.** *Hum Mol Genet* 2013, **22:**2462-2470.
10. Lee JM, Ramos EM, Lee JH, Gillis T, Mysore JS, Hayden MR, Warby SC, Morrison P, Nance M, Ross CA, et al: **CAG repeat expansion in Huntington disease determines age at onset in a fully dominant fashion.** *Neurology* 2012, **78:**690-695.
11. Gusella JF, MacDonald ME, Lee JM: **Genetic modifiers of Huntington's disease.** *Movement disorders : official journal of the Movement Disorder Society* 2014, **29:**1359-1365.
12. Zuccato C, Cattaneo E: **Role of brain-derived neurotrophic factor in Huntington's disease.** *Prog Neurobiol* 2007, **81:**294-330.

13. Baydyuk M, Xu B: **BDNF signaling and survival of striatal neurons.** *Frontiers in cellular neuroscience* 2014, **8:**254.
14. Minichiello L: **TrkB signalling pathways in LTP and learning.** *Nature reviews Neuroscience* 2009, **10:**850-860.
15. Panja D, Bramham CR: **BDNF mechanisms in late LTP formation: A synthesis and breakdown.** *Neuropharmacology* 2014, **76 Pt C:**664-676.
16. Leal G, Bramham CR, Duarte CB: **BDNF and Hippocampal Synaptic Plasticity.** *Vitam Horm* 2017, **104:**153-195.
17. Carvalho AL, Caldeira MV, Santos SD, Duarte CB: **Role of the brain-derived neurotrophic factor at glutamatergic synapses.** *British journal of pharmacology* 2008, **153 Suppl 1:**S310-324.
18. Afonso P, De Luca P, Carvalho RS, Cortes L, Pinheiro P, Oliveiros B, Almeida RD, Mele M, Duarte CB: **BDNF increases synaptic NMDA receptor abundance by enhancing the local translation of Pyk2 in cultured hippocampal neurons.** *Sci Signal* 2019, **12:**eaav3577.
19. Crozier RA, Black IB, Plummer MR: **Blockade of NR2B-containing NMDA receptors prevents BDNF enhancement of glutamatergic transmission in hippocampal neurons.** *Learning & memory (Cold Spring Harbor, NY)* 1999, **6:**257-266.
20. Hofer M, Pagliusi SR, Hohn A, Leibrock J, Barde YA: **Regional distribution of brain-derived neurotrophic factor mRNA in the adult mouse brain.** *The EMBO journal* 1990, **9:**2459-2464.
21. Altar CA, Cai N, Bliven T, Juhasz M, Conner JM, Acheson AL, Lindsay RM, Wiegand SJ: **Anterograde transport of brain-derived neurotrophic factor and its role in the brain.** *Nature* 1997, **389:**856-860.
22. Baquet ZC, Gorski JA, Jones KR: **Early striatal dendrite deficits followed by neuron loss with advanced age in the absence of anterograde cortical brain-derived neurotrophic factor.** *The Journal of neuroscience : the official journal of the Society for Neuroscience* 2004, **24:**4250-4258.
23. Canals JM, Pineda JR, Torres-Peraza JF, Bosch M, Martín-Ibañez R, Muñoz MT, Mengod G, Ernfors P, Alberch J: **Brain-derived neurotrophic factor regulates the onset and severity of motor dysfunction associated with enkephalinergic neuronal degeneration in Huntington's disease.** *The Journal of neuroscience : the official journal of the Society for Neuroscience* 2004, **24:**7727-7739.
24. Zuccato C, Marullo M, Conforti P, MacDonald ME, Tartari M, Cattaneo E: **Systematic assessment of BDNF and its receptor levels in human cortices affected by Huntington's disease.** *Brain pathology (Zurich, Switzerland)* 2008, **18:**225-238.
25. Brito V, Puigdellívol M, Giralt A, del Toro D, Alberch J, Ginés S: **Imbalance of p75(NTR)/TrkB protein expression in Huntington's disease: implication for neuroprotective therapies.** *Cell death & disease* 2013, **4:**e595.
26. Gharami K, Xie Y, An JJ, Tonegawa S, Xu B: **Brain-derived neurotrophic factor over-expression in the forebrain ameliorates Huntington's disease phenotypes in mice.** *J Neurochem* 2008, **105:**369-379.
27. Xie Y, Hayden MR, Xu B: **BDNF overexpression in the forebrain rescues Huntington's disease phenotypes in YAC128 mice.** *The Journal of neuroscience : the official journal of the Society for Neuroscience* 2010, **30:**14708-14718.
28. Nguyen KQ, Rymar VV, Sadikot AF: **Impaired TrkB Signaling Underlies Reduced BDNF-Mediated Trophic Support of Striatal Neurons in the R6/2 Mouse Model of Huntington's Disease.** *Frontiers in cellular neuroscience* 2016, **10:**37.
29. Li JL, Hayden MR, Almqvist EW, Brinkman RR, Durr A, Dodé C, Morrison PJ, Suchowersky O, Ross CA, Margolis RL, et al: **A genome scan for modifiers of age at onset in Huntington disease: The HD MAPS study.** *American journal of human genetics* 2003, **73:**682-687.

30. Wexler NS, Lorimer J, Porter J, Gomez F, Moskowitz C, Shackell E, Marder K, Penchaszadeh G, Roberts SA, Gayán J, et al: **Venezuelan kindreds reveal that genetic and environmental factors modulate Huntington's disease age of onset.** *Proceedings of the National Academy of Sciences of the United States of America* 2004, **101:**3498-3503.
31. **Identification of Genetic Factors that Modify Clinical Onset of Huntington's Disease.** *Cell* 2015, **162:**516-526.
32. Chaves G, Stanley J, Pourmand N: **Mutant Huntingtin Affects Diabetes and Alzheimer's Markers in Human and Cell Models of Huntington's Disease.** *Cells* 2019, **8**.
33. Glerup S, Bolcho U, Molgaard S, Boggild S, Vaegter CB, Smith AH, Nieto-Gonzalez JL, Ovesen PL, Pedersen LF, Fjorback AN, et al: **SorCS2 is required for BDNF-dependent plasticity in the hippocampus.** *Mol Psychiatry* 2016, **21:**1740-1751.
34. Glerup S, Olsen D, Vaegter CB, Gustafsen C, Sjoegaard SS, Hermey G, Kjolby M, Molgaard S, Ulrichsen M, Boggild S, et al: **SorCS2 Regulates Dopaminergic Wiring and Is Processed into an Apoptotic Two-Chain Receptor in Peripheral Glia.** *Neuron* 2014, **82:**1074-1087.
35. Olsen D, Wellner N, Kaas M, de Jong IEM, Sotty F, Didriksen M, Glerup S, Nykjaer A: **Altered dopaminergic firing pattern and novelty response underlie ADHD-like behavior of SorCS2-deficient mice.** *Transl Psychiatry* 2021, **11:**74.
36. Malik AR, Willnow TE: **VPS10P Domain Receptors: Sorting Out Brain Health and Disease.** *Trends Neurosci* 2020, **43:**870-885.
37. Glerup S, Olsen D, Vaegter CB, Gustafsen C, Sjoegaard SS, Hermey G, Kjolby M, Molgaard S, Ulrichsen M, Boggild S, et al: **SorCS2 regulates dopaminergic wiring and is processed into an apoptotic two-chain receptor in peripheral glia.** *Neuron* 2014, **82:**1074-1087.
38. Mangiarini L, Sathasivam K, Seller M, Cozens B, Harper A, Hetherington C, Lawton M, Trottier Y, Lehrach H, Davies SW, Bates GP: **Exon 1 of the HD gene with an expanded CAG repeat is sufficient to cause a progressive neurological phenotype in transgenic mice.** *Cell* 1996, **87:**493-506.
39. Tomé S, Manley K, Simard JP, Clark GW, Slean MM, Swami M, Shelbourne PF, Tillier ER, Monckton DG, Messer A, Pearson CE: **MSH3 polymorphisms and protein levels affect CAG repeat instability in Huntington's disease mice.** *PLoS genetics* 2013, **9:**e1003280.
40. Hawes SL, Gillani F, Evans RC, Benkert EA, Blackwell KT: **Sensitivity to theta-burst timing permits LTP in dorsal striatal adult brain slice.** *Journal of neurophysiology* 2013, **110:**2027-2036.
41. López-Benito S, Sánchez-Sánchez J, Brito V, Calvo L, Lisa S, Torres-Valle M, Palko ME, Vicente-García C, Fernández-Fernández S, Bolaños JP, et al: **Regulation of BDNF Release by ARMS/Kidins220 through Modulation of Synaptotagmin-IV Levels.** *The Journal of neuroscience : the official journal of the Society for Neuroscience* 2018, **38:**5415-5428.
42. Sahu MP, Nikkilä O, Lågas S, Kolehmainen S, Castrén E: **Culturing primary neurons from rat hippocampus and cortex.** *Neuronal Signal* 2019, **3:**Ns20180207.
43. Fred SM, Laukkanen L, Brunello CA, Vesa L, Göös H, Cardon I, Moliner R, Maritzen T, Varjosalo M, Casarotto PC, Castrén E: **Pharmacologically diverse antidepressants facilitate TRKB receptor activation by disrupting its interaction with the endocytic adaptor complex AP-2.** *The Journal of biological chemistry* 2019, **294:**18150-18161.
44. Rezgaoui M, Hermey G, Riedel IB, Hampe W, Schaller HC, Hermans-Borgmeyer I: **Identification of SorCS2, a novel member of the VPS10 domain containing receptor family, prominently expressed in the developing mouse brain.** *Mech Dev* 2001, **100:**335-338.
45. Lovinger DM: **Neurotransmitter roles in synaptic modulation, plasticity and learning in the dorsal striatum.** *Neuropharmacology* 2010, **58:**951-961.
46. Gerfen CR, Surmeier DJ: **Modulation of striatal projection systems by dopamine.** *Annu Rev Neurosci* 2011, **34:**441-466.

47. Ehrlich ME: **Huntington's disease and the striatal medium spiny neuron: cell-autonomous and non-cell-autonomous mechanisms of disease.** *Neurotherapeutics* 2012, **9:**270-284.
48. Ginés S, Bosch M, Marco S, Gavaldà N, Díaz-Hernández M, Lucas JJ, Canals JM, Alberch J: **Reduced expression of the TrkB receptor in Huntington's disease mouse models and in human brain.** *The European journal of neuroscience* 2006, **23:**649-658.
49. Knüsel B, Rabin SJ, Hefti F, Kaplan DR: **Regulated neurotrophin receptor responsiveness during neuronal migrationand early differentiation.** *The Journal of neuroscience : the official journal of the Society for Neuroscience* 1994, **14:**1542-1554.
50. Di Lieto A, Rantamäki T, Vesa L, Yanpallewar S, Antila H, Lindholm J, Rios M, Tessarollo L, Castrén E: **The responsiveness of TrkB to BDNF and antidepressant drugs is differentially regulated during mouse development.** *PloS one* 2012, **7:**e32869.
51. Guo W, Nagappan G, Lu B: **Differential effects of transient and sustained activation of BDNF-TrkB signaling.** *Developmental neurobiology* 2018, **78:**647-659.
52. Volianskis A, France G, Jensen MS, Bortolotto ZA, Jane DE, Collingridge GL: **Long-term potentiation and the role of N-methyl-D-aspartate receptors.** *Brain research* 2015, **1621:**5-16.
53. Lin SY, Wu K, Levine ES, Mount HT, Suen PC, Black IB: **BDNF acutely increases tyrosine phosphorylation of the NMDA receptor subunit 2B in cortical and hippocampal postsynaptic densities.** *Brain research Molecular brain research* 1998, **55:**20-27.
54. Xu F, Plummer MR, Len GW, Nakazawa T, Yamamoto T, Black IB, Wu K: **Brain-derived neurotrophic factor rapidly increases NMDA receptor channel activity through Fyn-mediated phosphorylation.** *Brain research* 2006, **1121:**22-34.
55. Otis JM, Fitzgerald MK, Mueller D: **Infralimbic BDNF/TrkB enhancement of GluN2B currents facilitates extinction of a cocaine-conditioned place preference.** *The Journal of neuroscience : the official journal of the Society for Neuroscience* 2014, **34:**6057-6064.
56. Smith-Dijak AI, Sepers MD, Raymond LA: **Alterations in synaptic function and plasticity in Huntington disease.** *J Neurochem* 2019, **150:**346-365.
57. Mitre M, Mariga A, Chao MV: **Neurotrophin signalling: novel insights into mechanisms and pathophysiology.** *Clinical science (London, England : 1979)* 2017, **131:**13-23.
58. Milnerwood AJ, Raymond LA: **Early synaptic pathophysiology in neurodegeneration: insights from Huntington's disease.** *Trends Neurosci* 2010, **33:**513-523.
59. Puigdellívol M, Cherubini M, Brito V, Giralt A, Suelves N, Ballesteros J, Zamora-Moratalla A, Martín ED, Eipper BA, Alberch J, Ginés S: **A role for Kalirin-7 in corticostriatal synaptic dysfunction in Huntington's disease.** *Hum Mol Genet* 2015, **24:**7265-7285.
60. Jia Y, Gall CM, Lynch G: **Presynaptic BDNF promotes postsynaptic long-term potentiation in the dorsal striatum.** *The Journal of neuroscience : the official journal of the Society for Neuroscience* 2010, **30:**14440-14445.
61. Li W, Pozzo-Miller L: **Differences in GluN2B-Containing NMDA Receptors Result in Distinct Long-Term Plasticity at Ipsilateral versus Contralateral Cortico-Striatal Synapses.** *eNeuro* 2019, **6**.
62. Suen PC, Wu K, Levine ES, Mount HT, Xu JL, Lin SY, Black IB: **Brain-derived neurotrophic factor rapidly enhances phosphorylation of the postsynaptic N-methyl-D-aspartate receptor subunit 1.** *Proceedings of the National Academy of Sciences of the United States of America* 1997, **94:**8191-8195.
63. Mizuno M, Yamada K, He J, Nakajima A, Nabeshima T: **Involvement of BDNF receptor TrkB in spatial memory formation.** *Learning & memory (Cold Spring Harbor, NY)* 2003, **10:**108-115.
64. Ma Q, Yang J, Milner TA, Vonsattel JG, Palko ME, Tessarollo L, Hempstead BL: **SorCS2-mediated NR2A trafficking regulates motor deficits in Huntington's disease.** *JCI insight* 2017, **2**.

933 65. Ayton S, Lei P, Appukuttan AT, Renoir T, Foliaki S, Chen F, Adlard PA, Hannan AJ, Bush AI: **Brain**
934 **Zinc Deficiency Exacerbates Cognitive Decline in the R6/1 Model of Huntington's Disease.**
935 *Neurotherapeutics* 2020, **17:**243-251.
936 66. Yang J, Ma Q, Dincheva I, Giza J, Jing D, Marinic T, Milner TA, Rajadhyaksha A, Lee FS,
937 Hempstead BL: **SorCS2 is required for social memory and trafficking of the NMDA receptor.**
938 *Mol Psychiatry* 2021, **26:**927-940.
939 67. Morella I, Hallum H, Brambilla R: **Dopamine D1 and Glutamate Receptors Co-operate With**
940 **Brain-Derived Neurotrophic Factor (BDNF) and TrkB to Modulate ERK Signaling in Adult**
941 **Striatal Slices.** *Frontiers in cellular neuroscience* 2020, **14:**564106.
942 68. Yang K, Trepanier C, Sidhu B, Xie YF, Li H, Lei G, Salter MW, Orser BA, Nakazawa T, Yamamoto T,
943 et al: **Metaplasticity gated through differential regulation of GluN2A versus GluN2B receptors**
944 **by Src family kinases.** *The EMBO journal* 2012, **31:**805-816.
945 69. Koch ET, Raymond LA: **Dysfunctional striatal dopamine signaling in Huntington's disease.**
946 *Journal of neuroscience research* 2019, **97:**1636-1654.
947 70. Visanji NP, Kamali Sarvestani I, Creed MC, Shams Shoaei Z, Nobrega JN, Hamani C, Hazrati LN:
948 **Deep brain stimulation of the subthalamic nucleus preferentially alters the translational**
949 **profile of striatopallidal neurons in an animal model of Parkinson's disease.** *Frontiers in cellular*
950 *neuroscience* 2015, **9:**221.
951 71. Andrew SE, Goldberg YP, Kremer B, Telenius H, Theilmann J, Adam S, Starr E, Squitieri F, Lin B,
952 Kalchman MA, et al.: **The relationship between trinucleotide (CAG) repeat length and clinical**
953 **features of Huntington's disease.** *Nature genetics* 1993, **4:**398-403.
954 72. Djoussé L, Knowlton B, Hayden M, Almqvist EW, Brinkman R, Ross C, Margolis R, Rosenblatt A,
955 Durr A, Dode C, et al: **Interaction of normal and expanded CAG repeat sizes influences age at**
956 **onset of Huntington disease.** *American journal of medical genetics Part A* 2003, **119a:**279-282.
957 73. Labadorf A, Hoss AG, Lagomarsino V, Latourelle JC, Hadzi TC, Bregu J, MacDonald ME, Gusella JF,
958 Chen JF, Akbarian S, et al: **RNA Sequence Analysis of Human Huntington Disease Brain Reveals**
959 **an Extensive Increase in Inflammatory and Developmental Gene Expression.** *PloS one* 2015,
960 **10:**e0143563.

961

962 # FIGURE LEGENDS

963 **Figure 1: SorCS2 is expressed by MSNs in corticostriatal circuits. a** RNA *In situ* hybridization shows *sorcs2*
964 expression in coronal section of P56 WT mouse brain, including the corticostriatal circuits. **b** Quantified
965 expression profile of *sorcs2* from the same section. Scale-bar is 700um. **c** *Sorcs2* is expressed in multiple
966 brain regions including induseum griseum (i.), interior cirgulate cortex (ii.), caudoputamen (iii.), lateral
967 septum (iv.), and piriform cortex (v.). **a-c** Image credit: ©2004 Allen Institute for Brain Science. Allen
968 Mouse Brain Atlas Available from mouse.brain-map.org/gene/show/57520. **d-e** Immunofluorescence
969 followed by confocal microscopy imaging revealed that SorCS2 is expressed by NeuN (**d**) and DARPP-32

970 (**e**) positive MSNs neurons in dorsal striatum of adult mice. Blue channel corresponds to nuclei stained by
971 Hoechst. The scale bar corresponds to 50µm, and to 20µm in magnified figures.

972 **Figure 2: SorCS2 accelerates and worsens HD disease progression. a** Rotarod motor skill learning in 12-
973 weeks-old males revealed contribution of genotype (p=0.014) and the trial number (p<0.0001) (two-way
974 ANOVA, WT: n=9, SorCS2 KO n=10). Repeated measurements one-way ANOVA and Tukey's multiple
975 comparisons test (MC): SorCS2 KO vs WT (p=0.0006), R6/1 vs WT (p<0.0001), SorCS2 KO; R6/1 vs WT
976 (p=0.0002), SorCS2 KO vs R6/1 (p=0.0154); **b-d** Staging of animals over time. WT; n=11, SorCS2 KO: n=10,
977 R6/1: n=12, SorCS2 KO;R6/1: n=13. **b** Body weight with contribution of genotype and age (both p<0.0001,
978 two-way ANOVA). MC: SorCS2 KO vs WT (p<0.0001), R6/1 vs WT males (p=0.0006), SorCS2 KO; R6/1 vs
979 R6/1 (p<0.0001), SorCS2 KO; R6/1 vs SorCS2 KO (p=0.0028). **c** Grip strength with contribution of genotype
980 (p=<0.0001) and age (p=0.0004) (two-way ANOVA). MC: R6/1 vs WT (p<0.0001). **d** Clasping score revealed
981 contribution of genotype (p<0.0001), age (p=0.0096), and genotype x age (p=0.0118) (two-way ANOVA).
982 MC: SorCS2 KO vs WT (p=0.0059), R6/1 vs WT (p<0.0001), SorCS2 KO; R6/1 vs WT (p<0.0001), SorCS2 KO;
983 R6/1 vs R6/1 (p<0.0001). **e** Representative visualization of gait patterns across genotypes. **f** Quantification
984 of the front limb stride length; p=0.0017 for difference among genotypes (one-way ANOVA), MC: WT vs
985 SorCS2 KO; R6/1 (p=0.0003), SorCS2 KO vs SorCS2 KO; R6/1 (p=0.003), R6/1 vs SorCS2 KO; R6/1 (0.0043)
986 (Fisher's LSD test). **g** Hind limb stride length; p=0.003 for difference among genotypes (one-way ANOVA),
987 MC: WT vs SorCS2 KO; R6/1 (p=0.0007), SorCS2 KO vs SorCS2 KO; R6/1 (p=0.0061), R6/1 vs SorCS2 KO;
988 R6/1 (p=0.0038) (Fisher's LSD test). **h** Hind limb base width; p=0.0061 for difference among genotypes
989 (one-way ANOVA). MC: WT vs SorCS2 KO; R6/1 (p=0.0009), SorCS2 KO vs SorCS2 KO; R6/1 (p=0.0141),
990 R6/1 vs SorCS2 KO; R6/1 (p=0.0133) (Fisher's LSD test). **i** Total distance traveled of 22-weeks-old males in
991 the open field test revealed significant contribution of the genotype (p<0.0001) (one-way ANOVA). MC:
992 WT vs R6/1 (p=0.0025), WT vs SorCS2 KO; R6/1 (p<0.0001), SorCS2 KO vs R6/1 (p=0.0018), SorCS2 KO vs

993 SorCS2 KO; R6/1 (p p<0.0001), R6/1 vs SorCS2 KO; R6/1 (p=0.009) (Fisher's LSD test). The graphs show
994 mean values ±SEM.

995 **Figure 3: Analysis of DARPP-32, TrkB, and SorCS2 protein levels in dorsal striatum of 22-weeks old males.**
996 **a** Immunoblot of SorCS2 protein levels in dorsal striatum of 22-weeks old males, quantified in (**b**) show
997 depleted levels of SorCS2 in R6/1 mice (p=0.0001). **c** Real-time qPCR analysis of SorCS2 expression in
998 dorsal striatum confirmed decreased levels of SorCS2 in R6/1 mice (p=0.0019); Unpaired two-tailed t-test
999 (**b-c**). **d** Representative immunoblots show detection of DARPP-32, the full-length (FL) and truncated (T.1)
1000 TrkB, and b-actin as loading control. Quantification of the immunoblots followed by ordinary one-way
1001 ANOVA and Tukey's multiple comparisons test revealed that SorCS2 KO have increased levels of FL-TrkB
1002 (p=0.0482) (**e**) but there were no changes in its truncated form (**f**). **g** Quantification of DARPP-32 show
1003 significant differences dependent on the genotype: R6/1 vs WT (p=0.0082), SorCS2 KO; R6/1 vs WT
1004 (p=0.0044), SorCS2 KO vs R6/1 (p<0.0001), SorCS2 KO; R6/1 vs SorCS2 KO (p<0.0001); Ordinary one-way
1005 ANOVA and Tukey's multiple comparisons test (**e-g**). RBI = Relative band intensity. Graphs show mean
1006 values ±SEM.

1007 **Figure 4: SorCS2 interaction with TrkB in dorsal striatum is required for TrkB phosphorylation upon**
1008 **BDNF stimulation. a** Representative western blot analysis of FL-TrkB co-immunoprecipitation (IP) with
1009 SorCS2 from dorsal striatum of adult WT mice. Pulldown using normal IgG from the same species serves
1010 as a negative control. SorCS2 physically binds TrkB in dorsal striatum. **b** Quantification of ELISA signal from
1011 rat primary cultures (E18, DIV10) treated with 10 ng/ml BDNF for 15 min shows increased interaction
1012 between TrkB and SorCS2 upon BDNF stimulation. **c** Representative western blot analysis of total and
1013 phosphorylated TrkB from acute brain slices of dorsal striatum from P5 pups stimulated with 50 ng/ml
1014 BDNF for 1 hour. b-actin serves as a loading control. **d** Quantification of the immunoblots (**c**). TrkB
1015 phosphorylation in WT samples and SorCS2 KO samples revealed significant differences (One-way ANOVA,
1016 p=0.0008). When treated with BDNF, WT samples show an increase in pTrkB phosphorylation (p=0.0023),

1017 while SorCS2 KO mice exhibit decreased phosphorylation (p=0.0047) (Multiple comparison test with
1018 Tukey's correction). The signal of pTrkB was normalized to total Full length TrkB. RBI = relative band
1019 intensity. Graphs show mean values ±SEM.

1020 **Figure 5: SorCS2 regulates BDNF-dependent LTP in dorsal striatum. a** Representative traces of
1021 input/output curves for each genotyped that were measured in dorsal striatum of P35-45 males. **b**
1022 Corticostriatal synapses of p35-45 males show no significant differences in AMPAR activity. Unpaired two-
1023 tailed t-test. WT: n=4 (16 slices), SorCS2 KO: n=4 (16 slices), R6/1: n=4 (14 slices), SorCS2 KO; R6/1: n=4
1024 (12 slices). **c** Induced LTP measurements in dorsal striatum of P35-45 males without treatment revealed
1025 impairments in SorCS2 KO and R6/1 models. Two-way ANOVA shows significant contribution of genotype
1026 and time (both p<0.0001). Kruskal-Wallis test and Dunn's multiple comparisons results: SorCS2 KO vs WT
1027 (p<0.0001), R6/1 vs WT (p<0.0001). WT: n=9, SorCS2 KO: n=9, R6/1: n=7. **d** Induced LTP measurements in
1028 dorsal striatum of P35-45 males treated with 10ng/ml BDNF. BDNF stimulation rescued the deficient LTP
1029 in SorCS2 KO but not in R6/1. We observe a decrease in WT due to oversaturation of the LTP induction
1030 during the experiment. Two-way ANOVA revealed significant contribution of genotype and time (both
1031 p<0.0001). Kruskal-Wallis test and Dunn's multiple comparisons results: SorCS2 KO vs WT (p<0.0001),
1032 R6/1 vs SorCS2 KO (p<0.0001). WT: n=8, SorCS2 KO: n=5, R6/1: n=6. **e-g** Comparison of the single
1033 genotypes –/+ BDNF. Two-way ANOVA revealed significant contribution of the genotype in (**e**) and (**f**) with
1034 p<0.0001, whereas R6/1 line shows no changes. **h** The violin plot visualizes the data for all conditions
1035 excluding the time factor and the baseline values. The data show significance p<0.0001 in Kruskal-Wallis
1036 test. Multiple-comparison testing is summarized in the table. **b-g** graphs show mean values ±SEM, **h** graph
1037 shows median with quartiles.

1038

1039 **Figure 6: HD aggravation depends on SorCS2 targeting of GluN2B at the postsynaptic densities prior**
1040 **BDNF stimulation. a** Field recordings of NMDA-R activity from *ex vivo* slices of dorsal striatum in P35-P45

1041 transgenic mice. DNQX is AMPAR inhibitor, RO 25-6981 is GluN2B inhibitor, and PEAQX is GluN2A inhibitor
1042 were added sequentially. Brown-Forsythe ANOVA test and multiple-comparison test (MC) with Welch's
1043 correction were used in (**b-e**). **b** Quantification of total NMDAR activity based on the field recordings show
1044 increased deficiency of NMDAR activity in the double-transgenic mice. ANOVA: p=0.0006; MC: SorCS2 KO
1045 vs WT (p=0.0309), R6/1 vs WT (p=0.0135), SorCS2 KO; R6/1 vs WT (p=0.0005), SorCS2 KO; R6/1 vs SorCS2
1046 KO (p=0.0127), SorCS2 KO; R6/1 vs R6/1 (p=0.0243). **c** Quantification of GluN2A activity shows that the
1047 NMDAR deficiency is not dependent on GluN2A. ANOVA: p=0.0236. MC: R6/1 vs WT (p=0.0288), SorCS2
1048 KO; R6/1 vs WT (p=0.0068). **d** Quantification of GluN2B activity revealed that deficient NMDAR activity is
1049 dependent of SorCS2-GluN2B functional interaction. ANOVA: p=0.0379; MC: SorCS2 KO vs WT (p=0.0191),
1050 SorCS2 KO; R6/1 vs WT (p=0.0194). **e** Quantification of super-resolution microscopy of GluN2B-PSD95 co-
1051 localization in *ex vivo* slices of dorsal striatum in presence or absence of BDNF. The results show that
1052 SorCS2 KO MSNs are deficient for GluN2B at the synapse, and they do not respond to BDNF stimulation.
1053 ANOVA: p=0.002, MC: WT-BDNF vs WT-vehicle (p=0.0339), SorCS2 KO-vehicle vs WT-vehicle (p=0.0214),
1054 SorCS2 KO-vehicle vs WT-BDNF (p=0.0053), SorCS2 KO-BDNF vs WT-BDNF (p=0.0088). **f** 3D reconstruction
1055 of the GluN2B (purple) co-localization (arrow) with PSD95 (yellow) at postsynaptic densities. The scale bar
1056 is 0.2 um. **g** Super-resolution Airyscan image of proximity ligation assay (PLA) for SorCS2-GluN2B
1057 interaction (in green) combined with immunofluorescence for PSD95 (in red) in *ex vivo* slices of dorsal
1058 striatum. Co-localization of SorCS2-GluN2B PLA signal with PSD95-positive objects are in blue
1059 (arrowhead). The scale bar is 1 um. **h** Quantification of SorCS2-GluN2B PLA signal in *ex vivo* slices of dorsal
1060 striatum treated with BDNF. There are fewer SorCS2-GluN2B protein complexes after BDNF stimulation.
1061 Welch's t-test: p=0.0011. **i** Quantification of the presence of SorCS2-GluN2B complexes in PSD95-positive
1062 postsynaptic densities. SorCS2-GluN2B complexes are abolished at postsynaptic density after BDNF
1063 stimulation. Welch's t-test: p=0.043.

1064 **Figure 7: A schematic model depicting the role of SorCS2 in neurotransmission of corticostriatal**
1065 **synapses. Step 1.** Upon BDNF release from cortical afferents, SorCS2 binds TrkB upon which they
1066 translocate to postsynaptic densities [33]. TrkB dimerization is strengthened by BDNF which is required
1067 for the robust phosphorylation of TrkB. **Step 2-3.** Activation of TrkB leads to dissociation of SorCS2 from
1068 GluN2B, possibly as consequence of GluN2B phosphorylation. **Step 4.** Once liberated from SorCS2, GluN2B
1069 is targeted to postsynaptic densities directly (displayed here) or after being in transit in the perisynapse
1070 (not displayed). **Step 5.** When GluN2B phosphorylation is not being maintained by BDNF, GluN2B will
1071 physically interact with SorCS2 in neuronal structures including postsynaptic densities. **Step 6-7.** SorCS2-
1072 GluN2B complexes may potentially be endocytosed into recycling vesicles following the lateral diffusion
1073 to the perisynapse.

1074

1075 ADDITIONAL MATERIALS

1076 **Supplementary Figure S1 (pdf):** SorCS2 is not expressed by interneurons in dorsal striatum.
1077 Immunofluorescence labelling four major interneuron populations in dorsal striatum followed by confocal
1078 microscopy. SorCS2 KO served as a negative control to which we calibrated the imaging settings. We used
1079 adult females for this analysis. **a** SorCS2 (in green) is not co-expressed in Calretinin (in red) interneurons.
1080 **b** SorCS2 is not expressed by large-aspiny cholinergic interneurons expressing ChaT. **c** SorCS2 is not
1081 expressed by GABAerfic fast-spiking parvalbumine-positive interneurons. **d** SorCS2 is not expressed by
1082 low-threshold-spiking NPY positive interneurons. Hoechst staining (in blue) labels the cell nuclei. The scale
1083 bar corresponds to 50µm, and to 20µm in magnified figures.

1084 **Supplementary Figure S2:** SorCS2 is not expressed by glial cells. Immunofluorescence labelling of SorCS2
1085 (in green) and GFAP+ glial cells (in red) in dorsal striatum followed by confocal microscopy. SorCS2 KO

1086 served as a negative control to which we calibrated the imaging settings. We used adult females for this
1087 analysis. Hoechst staining (in blue) labels the cell nuclei. The scale bar corresponds to 50µm, and to 20µm
1088 in magnified figures.

1089 **Supplementary Figure S3:** Physiological and behavior monitoring of transgenic HD mice including females.
1090 **a** Body weight in females with significant contribution of genotype and age (both p<0.0001, Mixed-effects
1091 model analysis with Tukey's correction). Repeated measurements one-way ANOVA and Tukey's multiple
1092 comparisons test: SorCS2 KO vs WT (p<0.0001), R6/1 vs WT (p<0.0001), SorCS2 KO; R6/1 vs WT
1093 (p<0.0001), R6/1 vs SorCS2 KO (p=0.0267), SorCS2 KO; R6/1 vs SorCS2 KO (p<0.0001), SorCS2 KO; R6/1 vs
1094 R6/1 (p<0.0001). **b** Grip strength in females with significant contribution of genotype (p<0.0001) and age
1095 (p=0.001) (Mixed-effects model analysis with Tukey's correction). Repeated measurements one-way
1096 ANOVA and Tukey's multiple comparisons test: SorCS2 KO vs WT (p=0.0441), R6/1 vs WT (p=0.0009),
1097 SorCS2 KO; R6/1 vs WT (p=0.0006), R6/1 vs SorCS2 KO (p<0.0001), SorCS2 KO; R6/1 vs SorCS2 KO
1098 (p<0.0001). **c** Clasping score in females with significant contribution of genotype and age (both p<0.0001,
1099 Mixed-effects model analysis with with Tukey's correction). Repeated measurements one-way ANOVA
1100 and Tukey's multiple comparisons test: SorCS2 KO vs WT (p<0.0001), R6/1 vs WT (p<0.0001), SorCS2 KO;
1101 R6/1 vs WT (p<0.0001), R6/1 vs SorCS2 KO (p=0.0003), SorCS2 KO; R6/1 vs SorCS2 KO (p<0.0001), SorCS2
1102 KO; R6/1 vs R6/1 (p<0.0001). **a-c** WT: n=10, SorCS2 KO: n=14, R6/1: n=16, SorCS2 KO; R6/1: n=8. **D** A built-
1103 in-house catwalk apparatus for a gait assay with a mouse inside of the corridor walking towards the box
1104 with the bedding. The paws reflect the green light. **e** Representative images of the gait from the different
1105 genotypes with decoded paws and visualized gait pattern. R6/1 have impaired gait which worsens in
1106 SorCS2 KO; R6/1 mice. RBI = Relative band intensity.

1107 **Supplementary Figure S4:** Protein analysis of cortex and dorsal striatum. **a** Representative immunoblot of
1108 SorCS2 and DARPP-32 in the dorsal striatum of P42-44 mice, which is quantified via densitometry of
1109 SorCS2 (**b**) and DARPP-32 (**c**) bands normalized to b-actin. We detected no differences in SorCS2 and

1110 DARPP-32 at this stage (unpaired two-tailed t-test). **d** Representative immunoblot showing SorCS2 protein
1111 levels in cortex of WT and R6/1 lines which do not differ quantified in **e** (unpaired two-tailed t-test). **f**
1112 Quantitative real-time PCR detects SorCS2 in cortex from 22-weeks-old mice. The expression is normalized
1113 to GAPDH transcripts serving as a housekeeping gene. There is no difference between WT and R6/1 line
1114 (unpaired two-tailed t-test). **g** BDNF levels in cortex from 22-week-old mice determined by ELISA. There is
1115 no significant differences between the genotypes (ordinary one-way ANOVA with Tukey's multiple
1116 comparisons test). **h** BDNF levels in dorsal striatum from 22-week-old mice determined by ELISA. We
1117 detected upregulated levels of BDNF in the double-transgenic HD model. Significant change in ordinary
1118 one-way ANOVA (p=0.0357). Tukey's multiple comparisons test: SorCS2 KO; R6/1 vs SorCS2 KO
1119 (p=0.0265). **i** Quantification of the ratio between proBDNF and BDNF levels was determined by
1120 densitometry of western blots in dorsal striatum from 22-week-old mice. There was no difference
1121 between the genotypes (ordinary one-way ANOVA with Tukey's multiple comparisons test). **j**
1122 Representative immunoblot of proBDNF and BDNF in dorsal striatum in 22-week-old mice. All graphs show
1123 mean with ±SEM.

1124 **Supplementary Figure S5:** Analysis of AMPAR and NMDAR activity in CA3-CA1 synapses of hippocampus.
1125 **a** Recordings of field potentials from CA3-CA1 synapses show no significant difference in AMPAR activity
1126 in regards to genotype (two-way ANOVA, WT: n=5, SorCS2 KO: n=8). Quantification of total NMDAR
1127 activity (**b**) and GluN2A activity (**c**) revealed no difference; however, SorCS2 KO mice have decreased
1128 GluN2B activity (p=0.0419) as shown in (**d**). Unpaired Welch's t-test. Mice were P21-22 of age. All graphs
1129 shows mean values ± SEM.

1130 **Supplementary Figure S6:** Analysis of selected synaptic proteins in homogenates and synaptosomes of
1131 dorsal striatum from P35 WT and SorCS2 KO mice. **a** Immunoblots of selected synaptic proteins in two
1132 distinct protein fractions. These data are quantified in the below graphs using densitometry and
1133 normalized to b-actin, followed by unpaired two-tailed t-test. We detect no difference in GluN1 (**b**),

1134 GluN2A (**c**) neither in GluN2B (**d**). As reported in Figure 3B, we detect upregulated levels of TrkB in the
1135 SorCS2 KO homogenate (**e**) (p=0.010742). We observe upregulation of PSD95 in SorCS2 KO homogenate
1136 (p=0.020426), however synaptosomes reflect normal levels of PSD95 (**f**). **g** Synaptophysin levels tend to
1137 decrease in SorCS2 KO homogenate and increase in synaptosomes, but there is no statistical significance.
1138 **h** We observe significant increase in total Erk1,2 in SorCS2 KO homogenate (p=0.0016), and a decrease in
1139 synaptosomes (p=0.008992). Mice were P35 of age. RBI = Relative band intensity. All graphs show mean
1140 ±SEM.

1141 **Supplementary video SV1: Representative video of gait assay result for WT mice walking through the**
1142 **catwalk assay.**

1143 **Supplementary video SV2: Representative video of SorCS2 KO mouse line walking through the catwalk**
1144 **assay.**

1145 **Supplementary video SV3: Representative video of R6/1 mouse line walking through the catwalk**
1146 **assay.**

1147 **Supplementary video SV4: Representative video of SorCS2 KO; R6/1 mouse line walking through the**
1148 **catwalk assay.**

1149

1150

1151 **Table 1: Overview of the statistical testing used in the study**

Data sets	Applied statistical tests	Corresponding figure
Rotarod motor skills	1. Two-way ANOVA, Tukey's correction 2. Repeated-measurements one-way ANOVA 3. Multiple comparison test with Tukey's correction	Figure 2a
Body weight	1. Two-way ANOVA (Mixed-effects model), Tukey's correction 2. Repeated-measurements one-way ANOVA 3. Multiple comparison test with Tukey's correction	Figure 2b, Suppl. Figure S3a

Grip strength	1. Two-way ANOVA (Mixed-effects model), Tukey's correction 2. Repeated-measurements one-way ANOVA 3. Multiple comparison test with Tukey's correction	Figure 2c, Suppl. Figure S3b
Clasping	1. Two-way ANOVA (Mixed-effects model), Tukey's correction 2. Repeated-measurements one-way ANOVA 3. Multiple comparison test with Tukey's correction	Figure 2d, Suppl. Figure S3c
Gait assay	1. Ordinary one-way ANOVA 2. Fisher's LSD multiple comparison test	Figure 2f-h
Open field test	1. Ordinary one-way ANOVA 2. Fisher's LSD multiple comparison test	Figure 2i
SorCS2 and DARPP-32 levels (two genotypes)	1. Unpaired two-tailed t-test	Figure 3b-c, Suppl. Figure S4b-c, S4e-f
Comparison of TrkB and DARPP-32 levels across genotypes	1. Ordinary one-way ANOVA 2. Multiple comparison test with Tukey's correction	Figure 3e-g, Suppl. Figure S4g-i
TrkB-SorCS2 ELISA	1. Unpaired two-tailed t-test	Figure 4b
TrkB phosphorylation in *ex vivo* slices	1. One-way ANOVA 2. Multi comparison test with Tukey's correction	Figure 4d
AMPAR activity in dorsal striatum	1. Two-way ANOVA (Mixed-effects model), Tukey's correction 2. Brown-Forsythe one-way ANOVA test 3. Multiple comparison test with Welch's correction	Figure 5b
AMPAR activity in hippocampus	1. Unpaired two-tailed t-test	Suppl. Figure S5a
LTP measurements	1. Two-way ANOVA, Tukey's correction 2. Kruskal-Wallis test 3. Multiple comparison test with Dunn's correction	Figure 5c-h
NMDAR activity in dorsal striatum (across genotypes)	1. Brown-Forsythe one-way ANOVA test 2. Multiple comparison test with Welch's correction	Figure 5b-d
NMDAR activity in hippocampus (two genotypes)	1. Unpaired t-test with Welch's correction	Suppl. Figure S5b-d

GluN2B-PSD95 co-localization	1. Brown-Forsythe one-way ANOVA test 2. Multiple comparison test with Welch's correction	Figure 5e
PLA assay	1. Unpaired t-test with Welch's correction	Figure 5h-i
Synaptosomes fractionation	1. Multiple unpaired t-test	Suppl. Figure S6b-k

1152

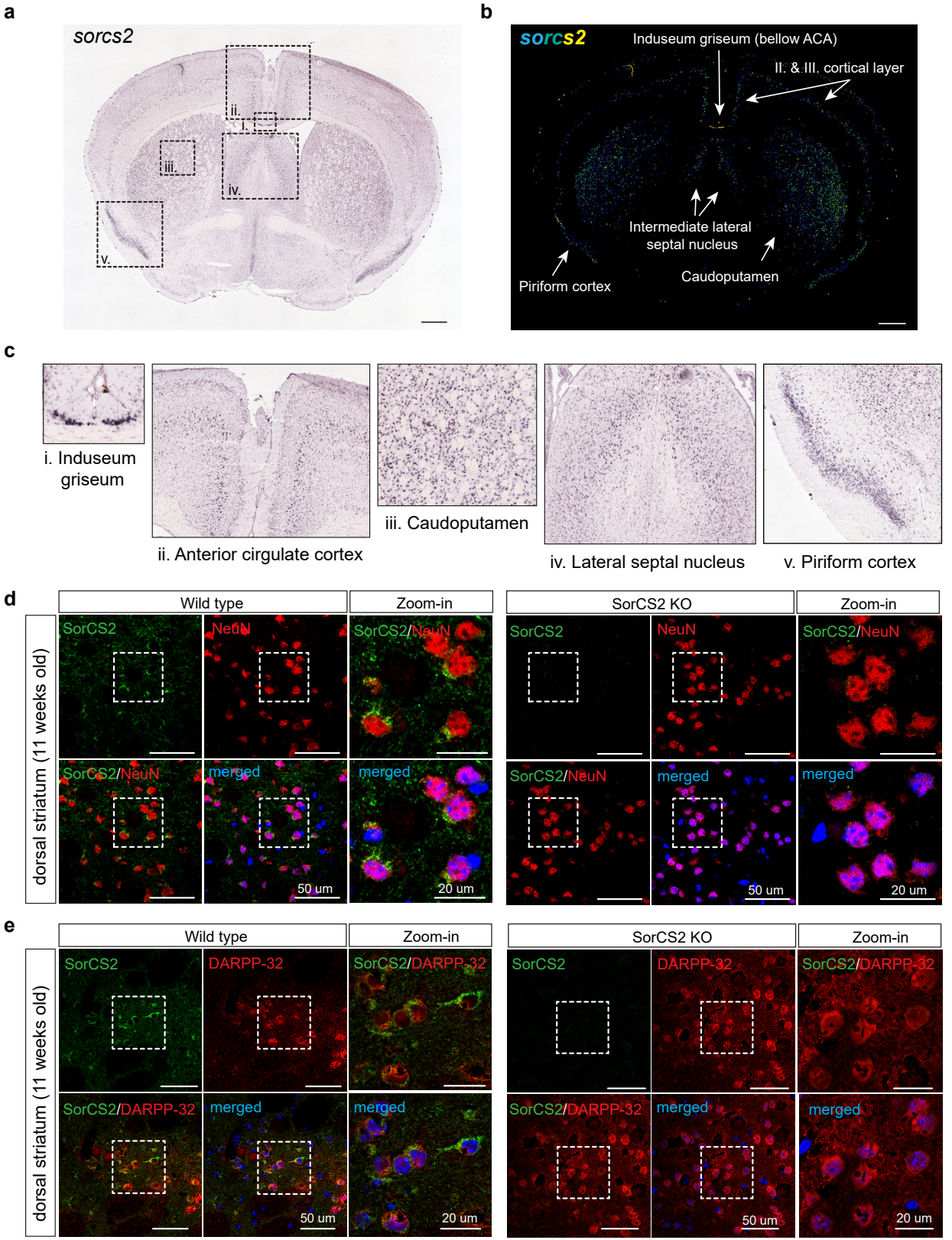
a
sorcs2
ii.
i.
iii.
iv.
v.
b
sorcs2
Induseum griseum (bellow ACA)
II. & III. cortical layer
Intermediate lateral
septal nucleus
Caudoputamen
Piriform cortex
c
i. Induseum
griseum
ii. Anterior cirgulate cortex
iii. Caudoputamen
iv. Lateral septal nucleus
v. Piriform cortex
d
Wild type
Zoom-in
SorCS2 KO
Zoom-in
dorsal striatum (11 weeks old)
SorCS2
NeuN
SorCS2/NeuN
merged
50 um
20 um
e
Wild type
Zoom-in
SorCS2 KO
Zoom-in
dorsal striatum (11 weeks old)
SorCS2
DARPP-32
SorCS2/DARPP-32
merged
50 um
20 um

Figure 1

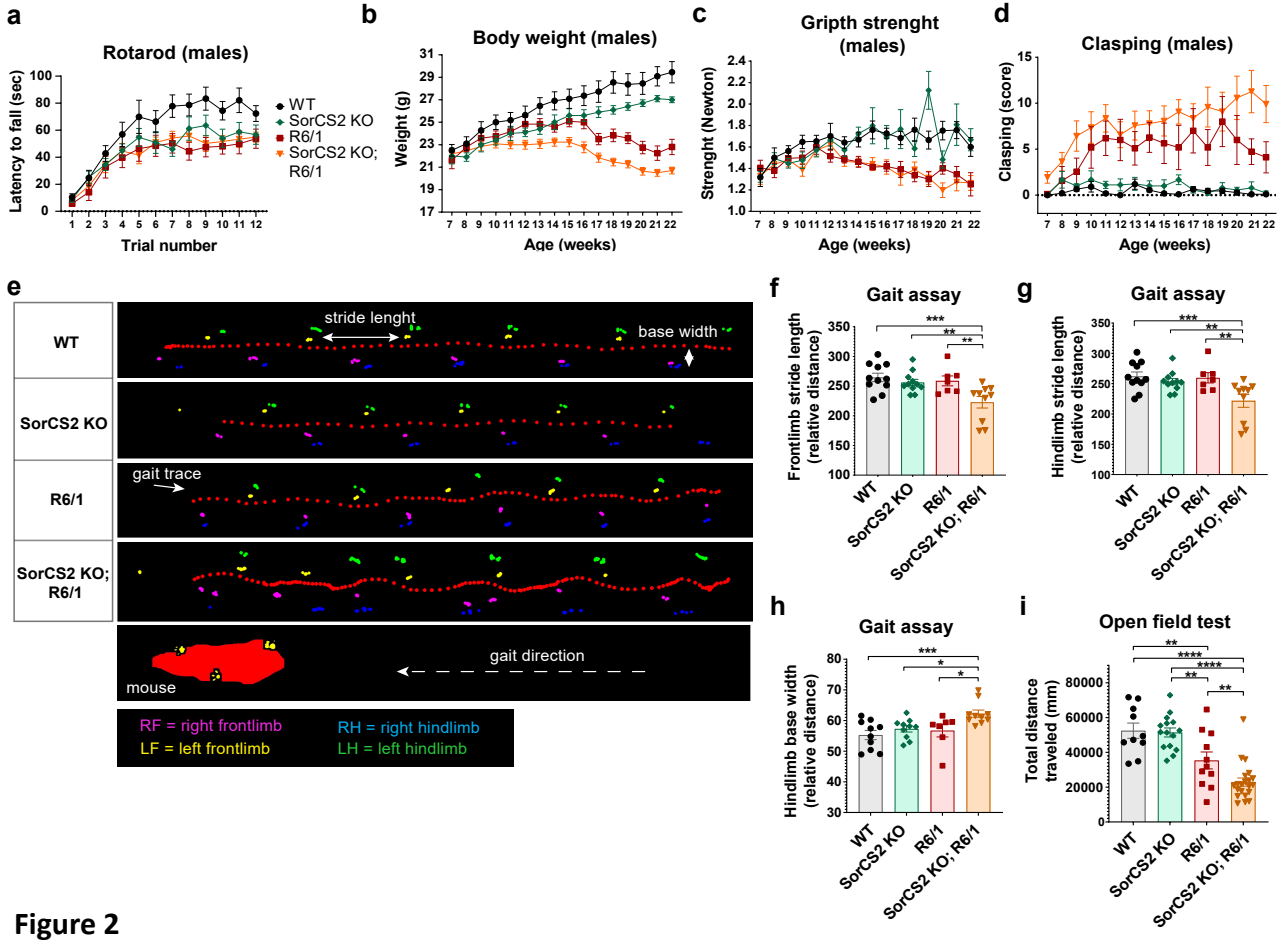
a
Rotarod (males)
Latency to fall (sec)
Trial number
WT
SorCS2 KO
R6/1
SorCS2 KO; R6/1
b
Body weight (males)
Weight (g)
Age (weeks)
c
Gripth strenght (males)
Strenght (Newton)
Age (weeks)
d
Clasping (males)
Clasping (score)
Age (weeks)
e
WT
SorCS2 KO
R6/1
SorCS2 KO; R6/1
stride lenght
base width
gait trace
gait direction
mouse
RF = right frontlimb
LF = left frontlimb
RH = right hindlimb
LH = left hindlimb
f
Gait assay
Frontlimb stride length (relative distance)
g
Gait assay
Hindlimb stride length (relative distance)
h
Gait assay
Hindlimb base width (relative distance)
i
Open field test
Total distance traveled (mm)

Figure 2

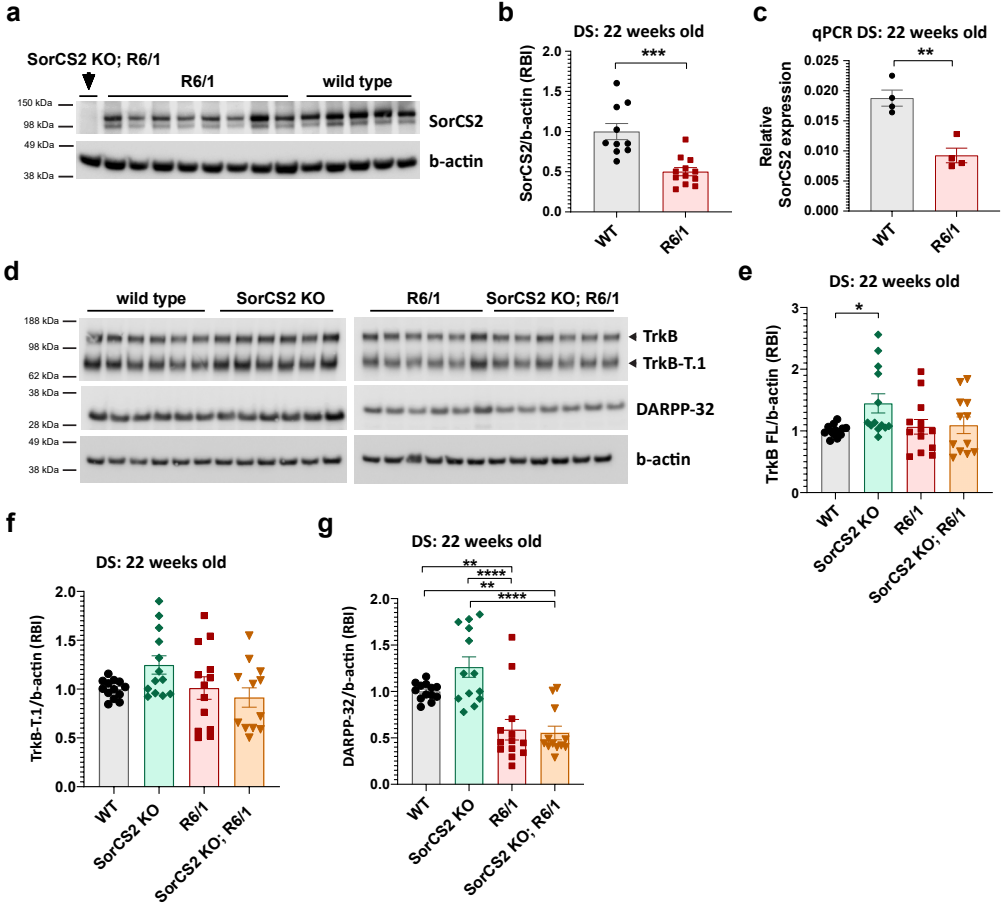
a
SorCS2 KO; R6/1
R6/1
wild type
150 kDa
98 kDa
49 kDa
38 kDa
SorCS2
b-actin
b
DS: 22 weeks old
SorCS2/b-actin (RBI)
***
WT
R6/1
c
qPCR DS: 22 weeks old
Relative SorCS2 expression
**
WT
R6/1
d
wild type
SorCS2 KO
R6/1
SorCS2 KO; R6/1
188 kDa
98 kDa
62 kDa
38 kDa
28 kDa
49 kDa
38 kDa
TrkB
TrkB-T.1
DARPP-32
b-actin
e
DS: 22 weeks old
TrkB FL/b-actin (RBI)
*
WT
SorCS2 KO
R6/1
SorCS2 KO; R6/1
f
DS: 22 weeks old
TrkB-T.1/b-actin (RBI)
WT
SorCS2 KO
R6/1
SorCS2 KO; R6/1
g
DS: 22 weeks old
DARPP-32/b-actin (RBI)
**
****
**
****
WT
SorCS2 KO
R6/1
SorCS2 KO; R6/1

Figure 3

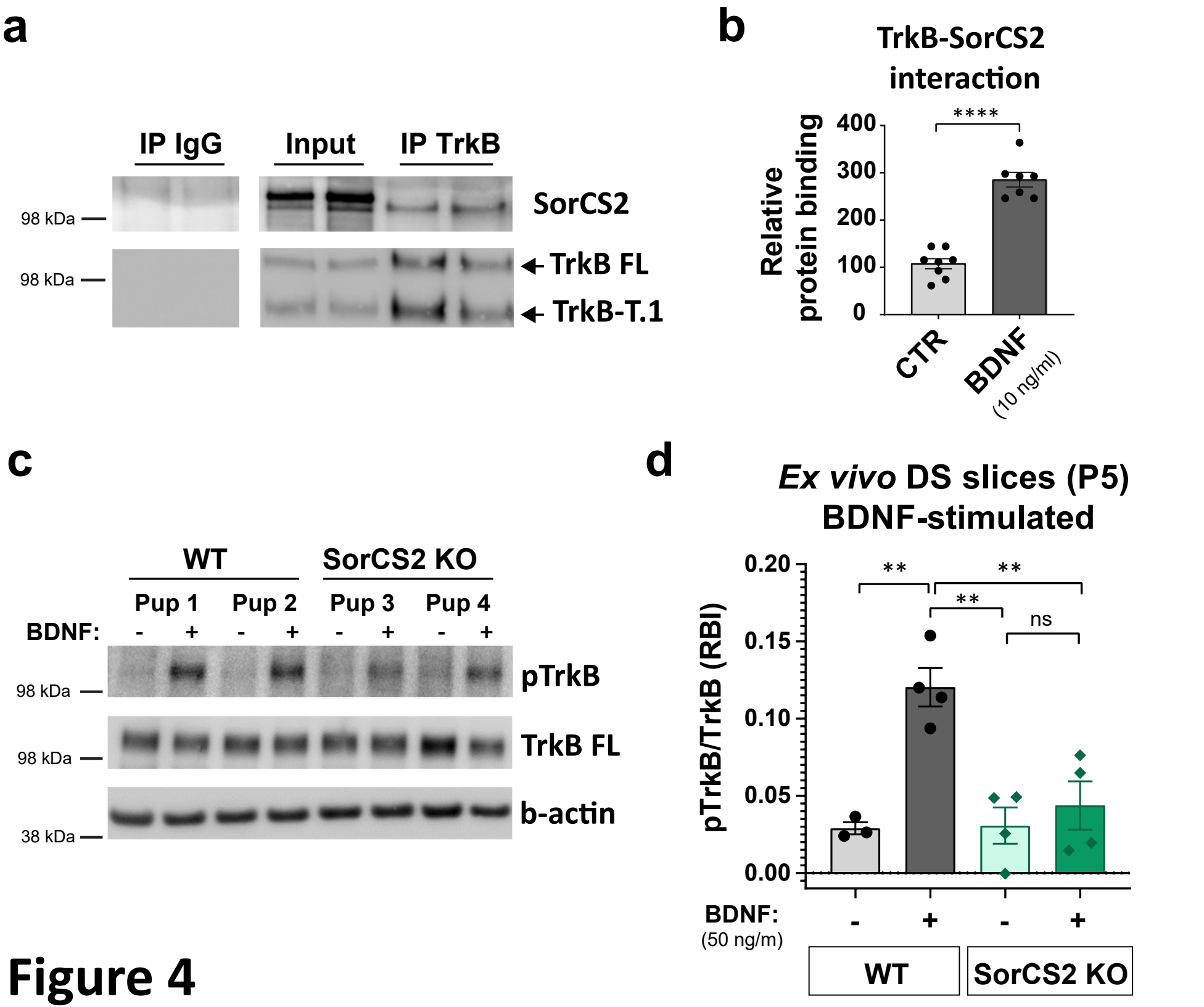
a
IP IgG
Input
IP TrkB
98 kDa
98 kDa
SorCS2
TrkB FL
TrkB-T.1
b
TrkB-SorCS2 interaction
Relative protein binding
400
300
200
100
0
****
CTR
BDNF
(10 ng/ml)
c
WT
SorCS2 KO
Pup 1
Pup 2
Pup 3
Pup 4
BDNF:
- + - + - + - +
98 kDa
98 kDa
38 kDa
pTrkB
TrkB FL
b-actin
d
Ex vivo DS slices (P5)
BDNF-stimulated
pTrkB/TrkB (RBI)
0.20
0.15
0.10
0.05
0.00
**
**
**
ns
BDNF:
(50 ng/m)
- + - +
WT
SorCS2 KO

Figure 4

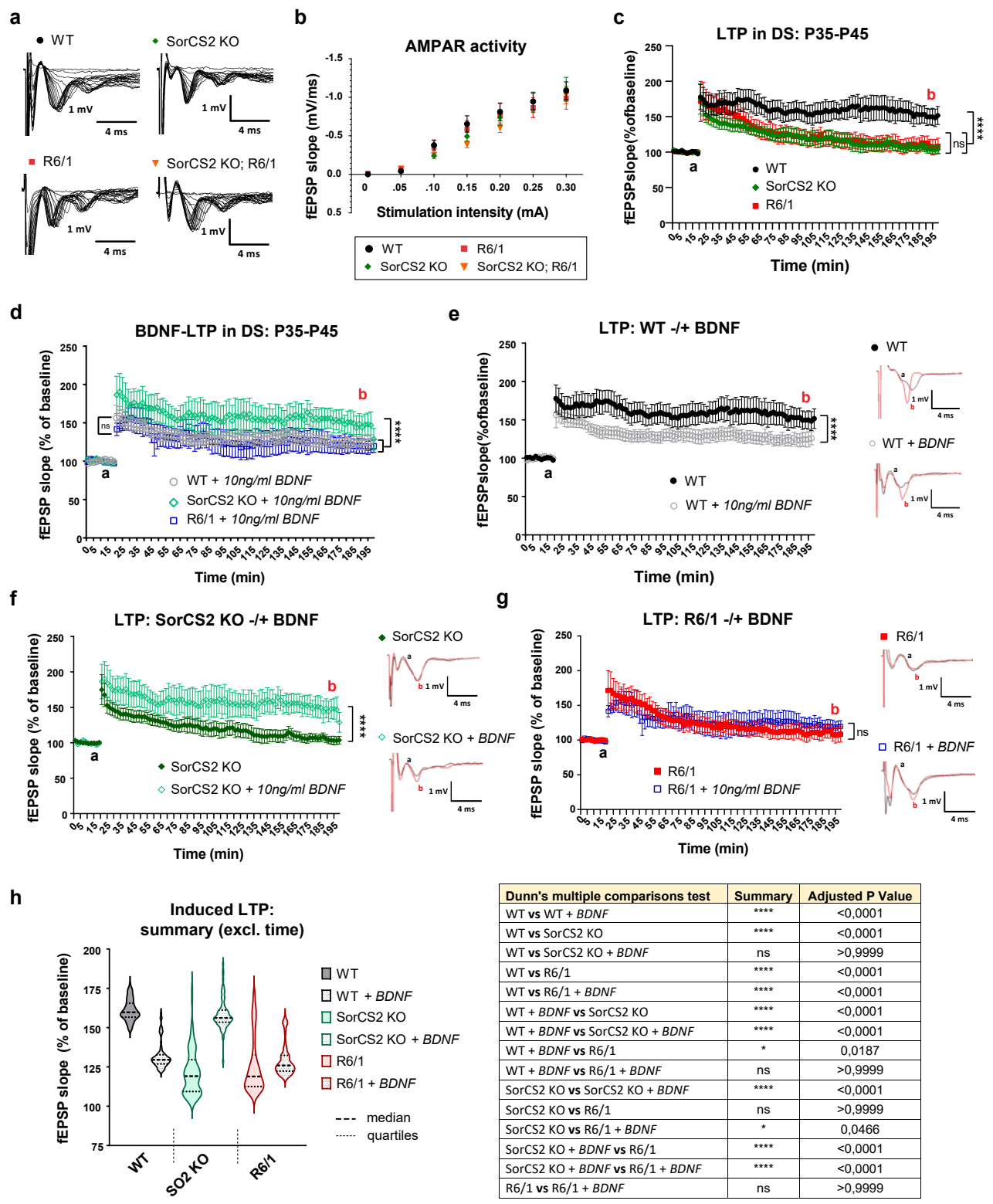

Dunn's multiple comparisons test	Summary	Adjusted P Value
WT **vs** WT + *BDNF*	****	<0,0001
WT **vs** SorCS2 KO	****	<0,0001
WT **vs** SorCS2 KO + *BDNF*	ns	>0,9999
WT **vs** R6/1	****	<0,0001
WT **vs** R6/1 + *BDNF*	****	<0,0001
WT + *BDNF* **vs** SorCS2 KO	****	<0,0001
WT + *BDNF* **vs** SorCS2 KO + *BDNF*	****	<0,0001
WT + *BDNF* **vs** R6/1	*	0,0187
WT + *BDNF* **vs** R6/1 + *BDNF*	ns	>0,9999
SorCS2 KO **vs** SorCS2 KO + *BDNF*	****	<0,0001
SorCS2 KO **vs** R6/1	ns	>0,9999
SorCS2 KO **vs** R6/1 + *BDNF*	*	0,0466
SorCS2 KO + *BDNF* **vs** R6/1	****	<0,0001
SorCS2 KO + *BDNF* **vs** R6/1 + *BDNF*	****	<0,0001
R6/1 **vs** R6/1 + *BDNF*	ns	>0,9999

Figure 5

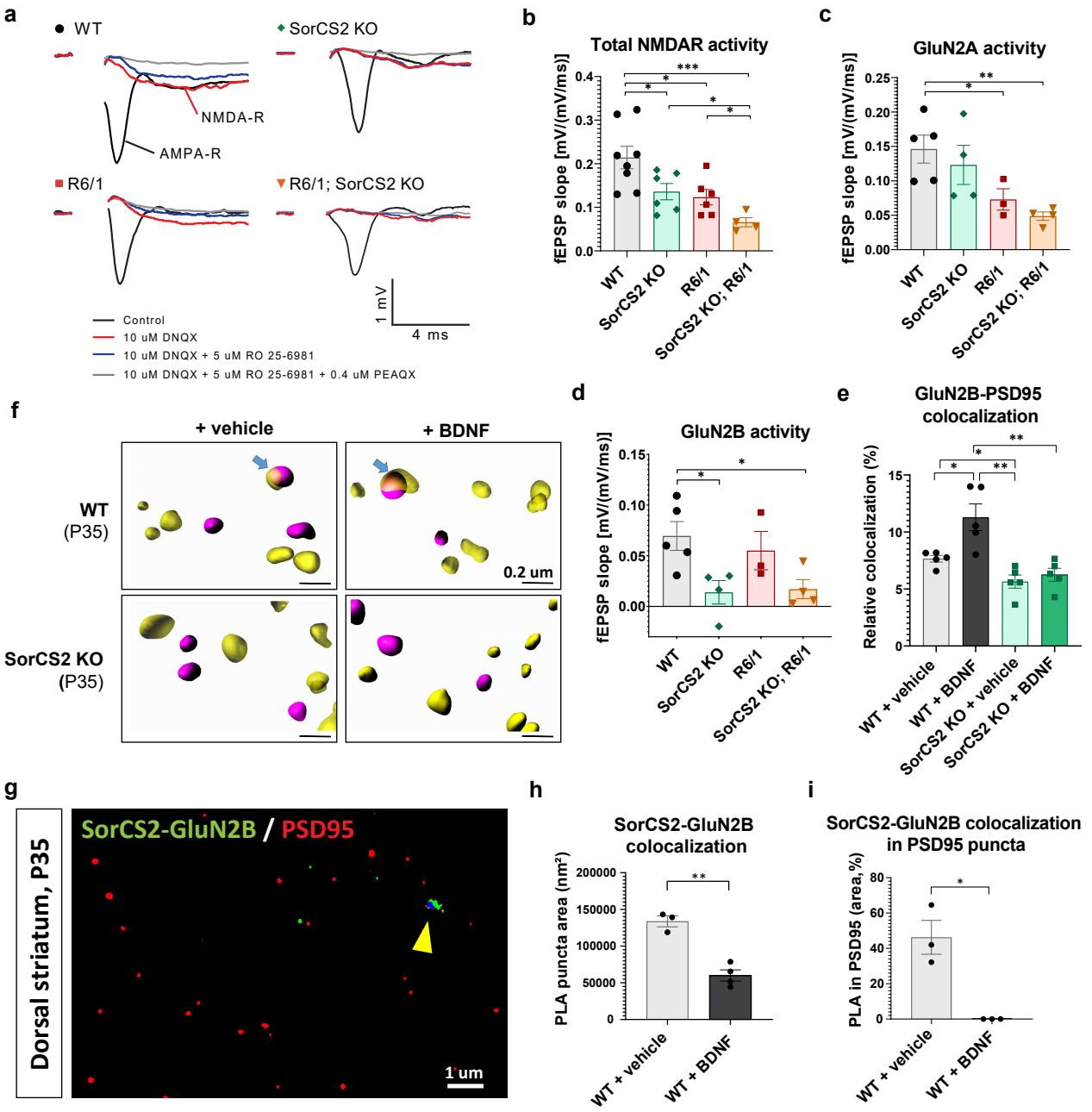
a
WT
SorCS2 KO
NMDA-R
AMPA-R
R6/1
R6/1; SorCS2 KO
1 mV
4 ms
Control
10 uM DNQX
10 uM DNQX + 5 uM RO 25-6981
10 uM DNQX + 5 uM RO 25-6981 + 0.4 uM PEAQX
b
Total NMDAR activity
fEPSP slope [mV/(mV/ms)]
WT
SorCS2 KO
R6/1
SorCS2 KO; R6/1
c
GluN2A activity
fEPSP slope [mV/(mV/ms)]
d
GluN2B activity
fEPSP slope [mV/(mV/ms)]
e
GluN2B-PSD95 colocalization
Relative colocalization (%)
WT + vehicle
WT + BDNF
SorCS2 KO + vehicle
SorCS2 KO + BDNF
f
+ vehicle
+ BDNF
WT (P35)
SorCS2 KO (P35)
0.2 um
g
Dorsal striatum, P35
SorCS2-GluN2B / PSD95
1 um
h
SorCS2-GluN2B colocalization
PLA puncta area (nm²)
i
SorCS2-GluN2B colocalization in PSD95 puncta
PLA in PSD95 (area,%)

Figure 6

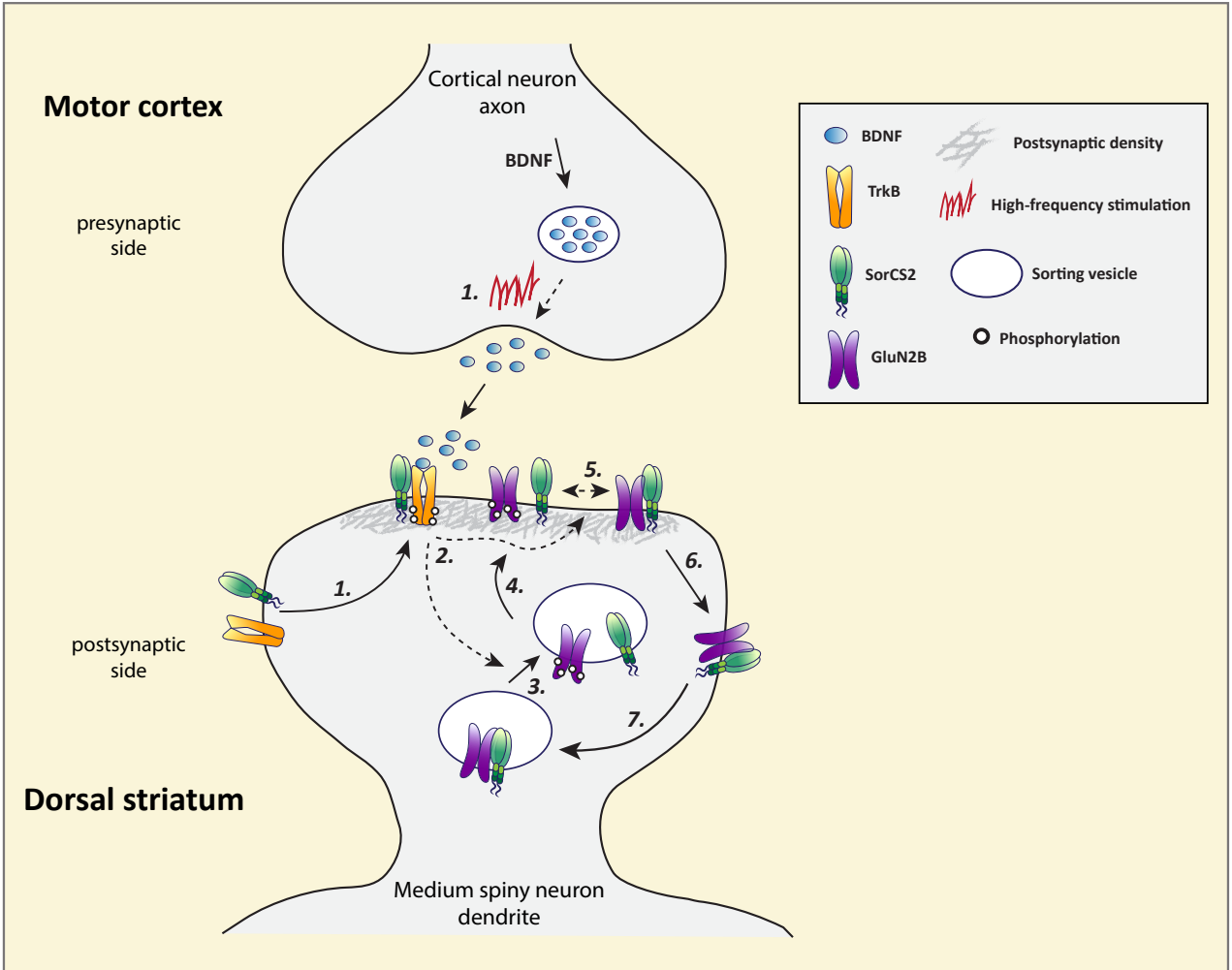
Motor cortex
Cortical neuron axon
BDNF
presynaptic side
1.
BDNF
TrkB
SorCS2
GluN2B
Postsynaptic density
High-frequency stimulation
Sorting vesicle
Phosphorylation
5.
2.
4.
6.
1.
postsynaptic side
3.
7.
Dorsal striatum
Medium spiny neuron dendrite

Figure 7

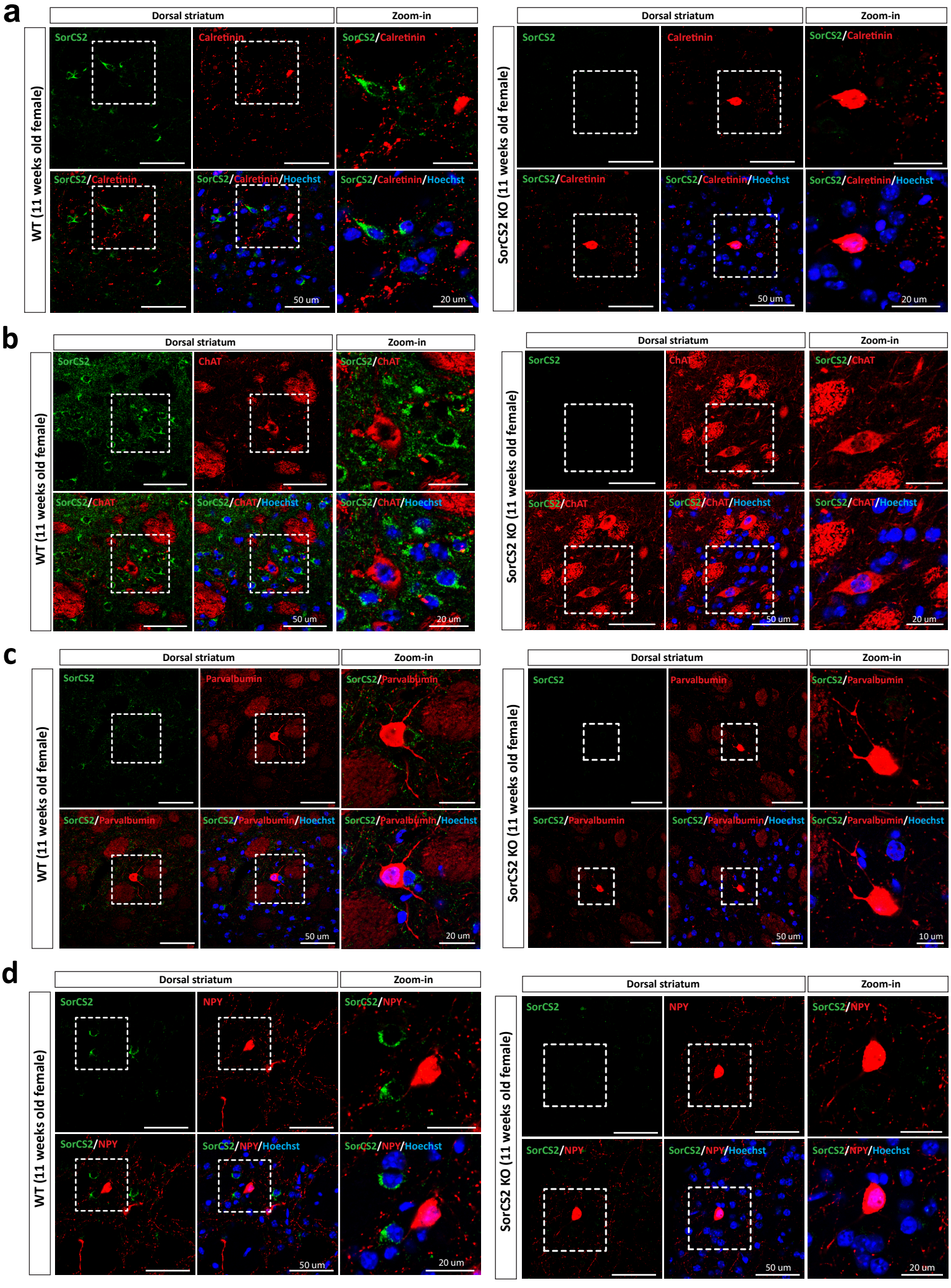

Supplementary Figure S1

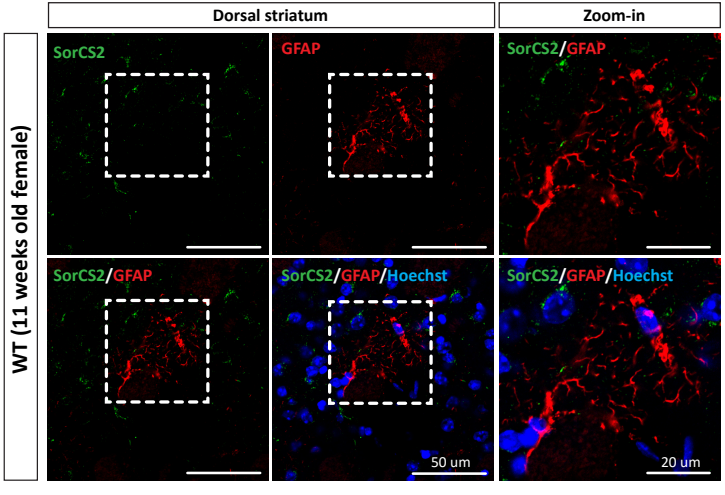

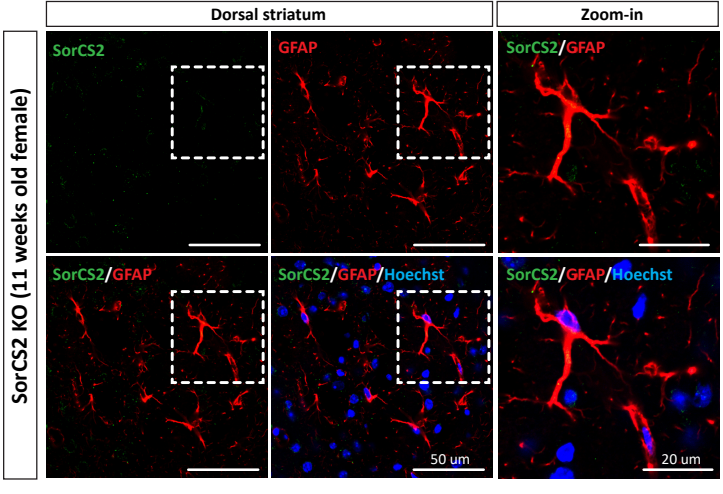

Supplementary Figure S2

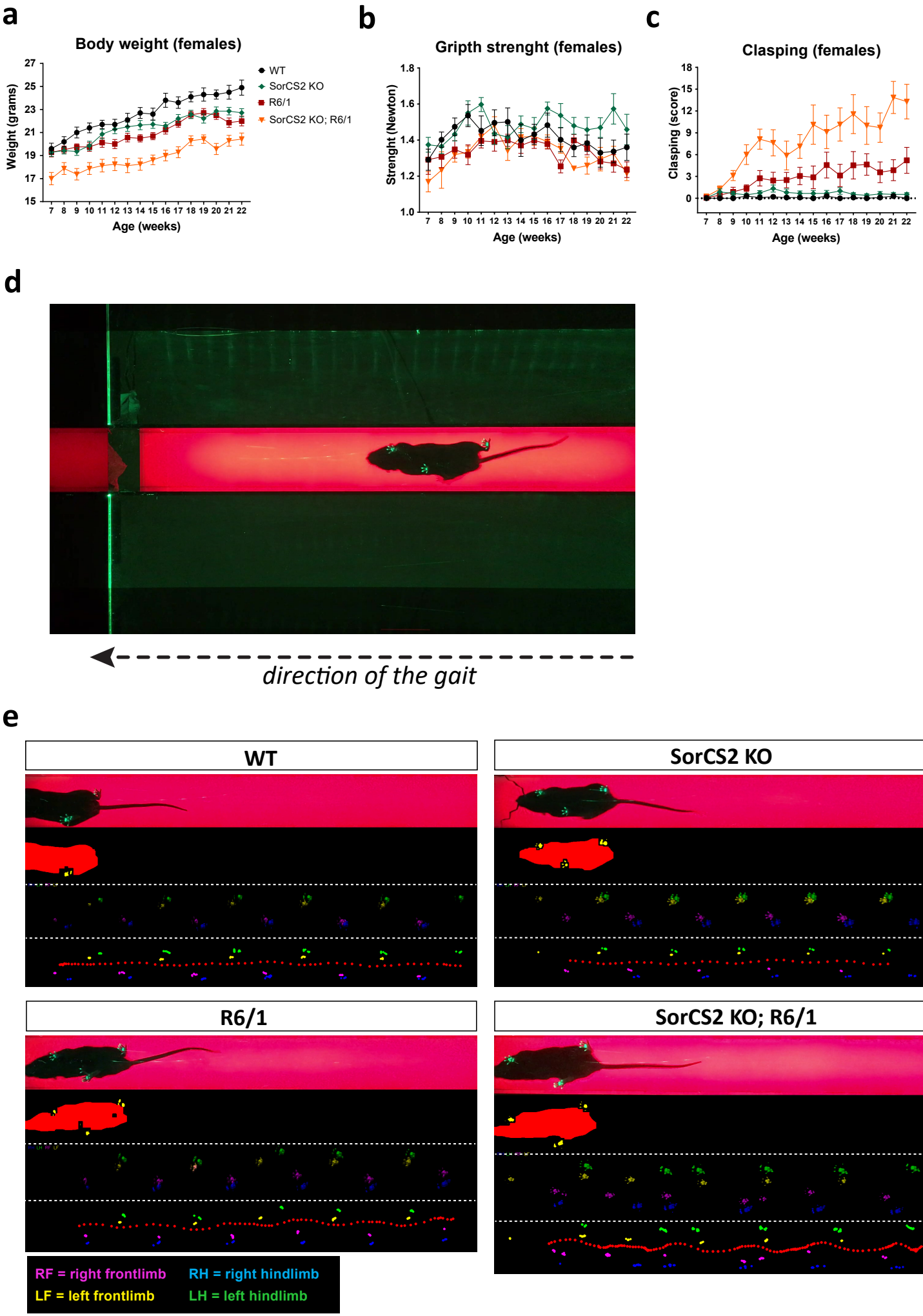

Supplementary Figure S3

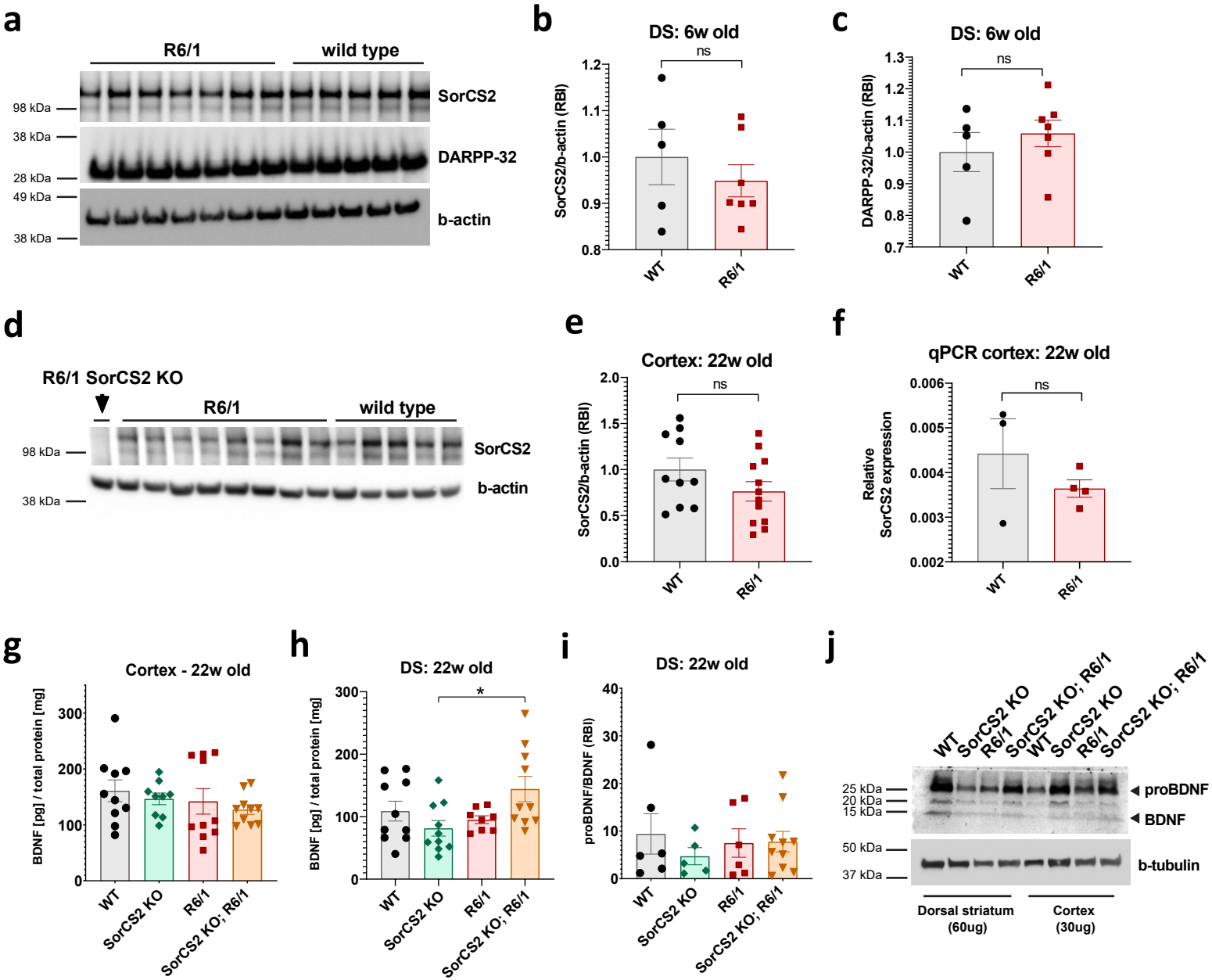

Supplementary Figure S4

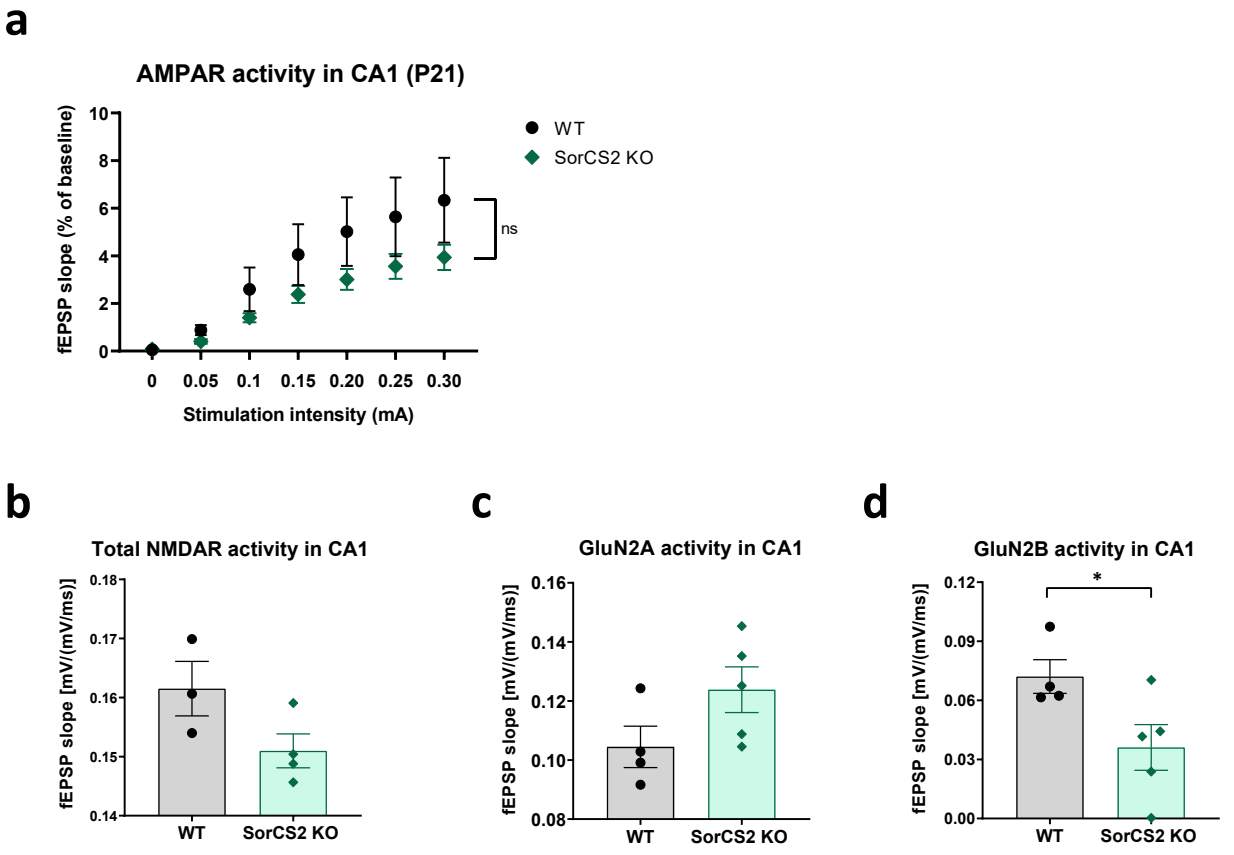

Supplementary Figure S5

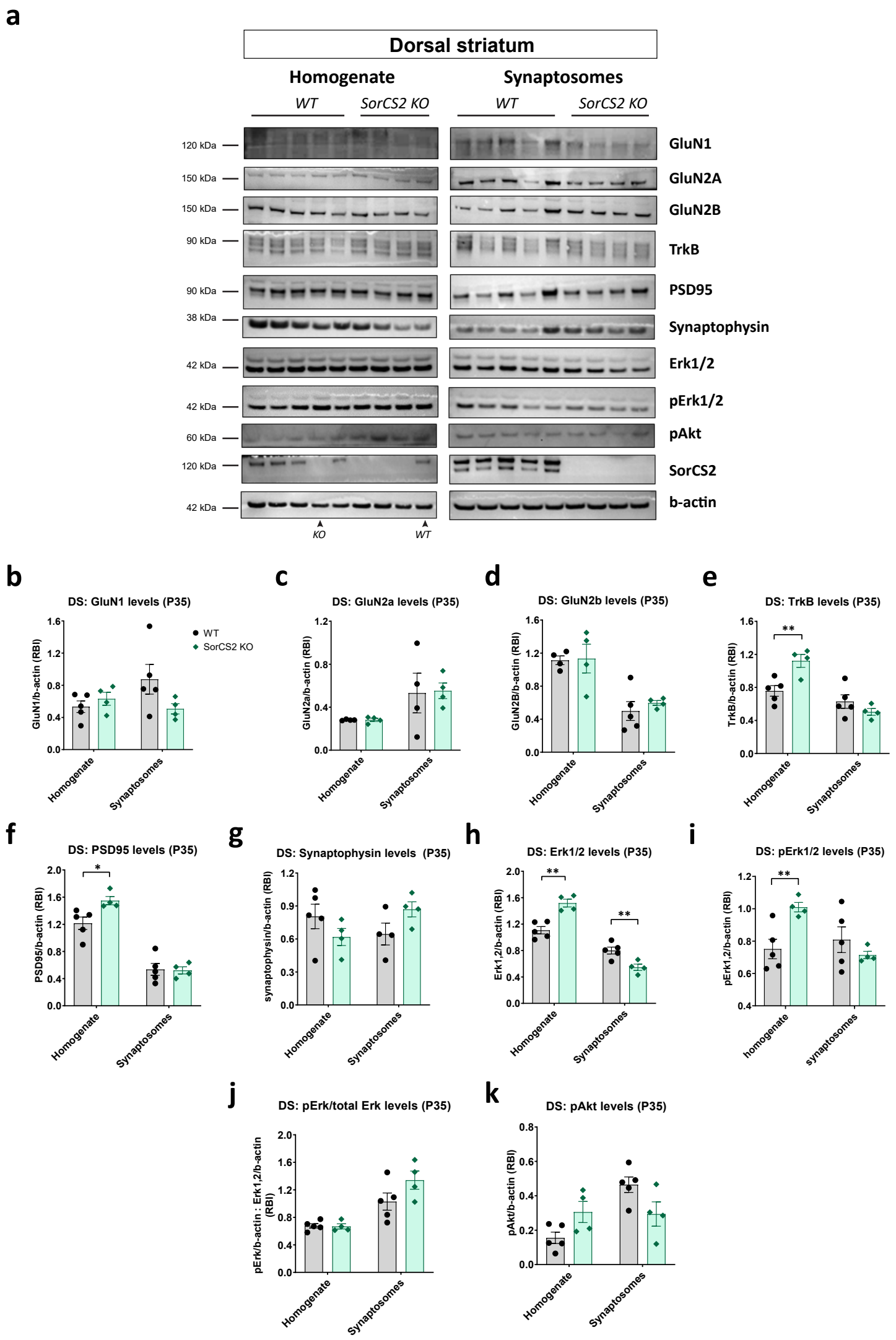

Supplementary Figure S6